

**TECHNICAL PAPER**

# Torsional strengthening of tubular type RC beams with NSM technique: Structural performance and cracking process using DIC

Chandan C. Gowda<sup>1</sup> | Joaquim A. O. Barros<sup>1</sup> | Maurizio Guadagnini<sup>2</sup> | Eduardo Pereira<sup>1</sup>

<sup>1</sup>ISISE, IBS, Department of Civil Engineering, University of Minho, Guimarães, Portugal

<sup>2</sup>Department of Civil and Structural Engineering, The University of Sheffield, Sheffield, UK

**Correspondence**

Chandan C. Gowda, IBS, Department of Civil Engineering, University of Minho, Campus de Azurém, Guimarães 4800 158, Portugal.  
Email: chandu627@gmail.com

**Funding information**

Foundation of Science and Technology: FCT, Grant/Award Numbers: SFRH/BD/129472/2017, PTDC/ECM-EST/1882/2014; Marie Curie Initial Training Network: ENDURE, Grant/Award Number: MC-ITN-2013-607851

**Abstract**

Despite the key role of thin-walled tubular reinforced concrete (RC) members in major critical infrastructure projects, for example, bridges, their torsional performance is still not well understood and the effectiveness of strengthening systems cannot be easily assessed, especially when using innovative strengthening materials. With a large part of critical infrastructure approaching its design service life, these issues are becoming more and more important. This paper examines the torsional behavior of thin-walled tubular RC beams and evaluates the contribution of different strengthening configurations using carbon fiber reinforced polymer (CFRP) reinforcement applied according to the near surface mounted (NSM) technique. Six strengthened specimens are tested with different amounts of CFRP laminates in the longitudinal and transverse direction. Digital image correlation (DIC) is used to gain a deeper understanding of the contribution of the NSM CFRP laminates to the fracture process and overall deformation behavior of the RC elements. The crack mouth opening displacement (CMOD) of the critical crack is compared to those of the other cracks, and the torsional crack evolution is assessed against the strain evolution in the CFRP laminates. The results confirm the effectiveness of NSM CFRP strengthening solutions for thin-walled RC members, and provide clear evidence that torsional performance can be improved in terms of torsional moment carrying capacity, torsional stiffness, torsional angle of rotation and limiting the crack width propagation, which improves the aggregate interlock shear resisting mechanism.

**KEYWORDS**

carbon fiber reinforced polymer laminate, digital image correlation, near surface mounted technique, torsional strengthening

Discussion on this paper must be submitted within two months of the print publication. The discussion will then be published in print, along with the authors' closure, if any, approximately nine months after the print publication.

## 1 | INTRODUCTION AND BACKGROUND

According to the European Construction Federation Industry (2014), about 320 bn euros were invested on

rehabilitation and maintenance in 2013 and this figure increased to 342 bn euros in 2017, showing the critical state of existing structures and infrastructure and highlighting the importance of developing efficient strengthening systems. Though several innovative solutions already exist to enhance the flexure and shear capacity of existing reinforced concrete (RC) elements, less attention has been paid to enhance the performance of key structural elements subjected to critical torsional forces (e.g., box girders, spandrel beams). With a large proportion of the existing infrastructure in Europe and across the world now reaching their service life or requiring rehabilitation and strengthening, reliable and durable solutions to increase their torsional capacity are therefore required.

The available strengthening methods for RC structures can be broadly divided into two categories (a) traditional strengthening methods, including span shortening or section enlargement,<sup>1</sup> shotcrete<sup>2</sup> or steel jacketing,<sup>3</sup> posttensioning,<sup>2</sup> and (b) innovative strengthening methods, typically comprising advanced fiber reinforced polymer (FRP) composites applied according to the externally bonded (EB) or the near surface mounted (NSM) techniques.

One of the first studies on the use of EBR FRP for torsional strengthening has been reported in,<sup>4</sup> where the authors investigated the effect of fiber orientation, number of strengthened faces, number of plies, as well as the use of anchorage systems. The use of 90° oriented fibers was found to provide better confinement and a higher increase in ultimate moment capacity, while continuous wrapping was found to provide higher ultimate strength and post cracking stiffness than individual strips. The use of EBR for the torsional strengthening of solid and box-section RC beams has been further investigated experimentally and numerically in References 5 and 6. Different strengthening configurations using both strips and continuous sheets were examined, and both solutions were found to improve torsional capacity and reduce crack propagation and evolution. Analytical formulations to predict the torsional capacity of the EBR FRP strengthened elements were also developed in References 5 and 7. In Reference 8, the performance of FRP strengthened RC T-beams subjected to combined torsion and shear was investigated.

More recently, the use of NSM FRP reinforcement for torsional strengthening was also examined.<sup>9,10</sup> In these studies, the authors examined the performance of NSM FRP laminates on solid section beams using both epoxy and cement based adhesives,<sup>9</sup> as well as the use of novel FRP ropes,<sup>10</sup> which were found to perform better in terms of torsional moment capacity than the more traditional laminates. FRP ropes are also explored for strengthening of RC deep beams in shear by embedded

through section (ETS) technique with and without anchorages in El-Saikaly et al.<sup>11</sup> and Chalioris et al.<sup>12</sup> In both references, the RC beams are strengthened with ETS along with different configurations, which involve CFRP sheets, CFRP L-strips with and without CFRP rope anchorage<sup>11</sup> and by CFRP ropes.<sup>12</sup> All the strengthened beams have increased shear capacity and more importantly, changed the brittle failure mode to a ductile flexural failure.

In comparison to EBR FRP, the use of NSM FRP reinforcement has many advantages, including ease of application, minimal aesthetic impact, better fire protection, reduced amount of surface preparation. In the case of shear and torsional strengthening, the effectiveness of EBR FRP is limited by premature delamination of the FRP material<sup>6</sup> due to stress concentration in the corners, which is unlikely to take place in NSM reinforcement as the laminates are inserted inside grooves in the concrete cover and can develop a much better bond with the concrete substrate.<sup>13,14</sup>

The present paper mainly explores the application of digital image correlation (DIC), a non-contact technique to assess the torsional behavior of beams strengthened with CFRP laminates. One of the early known applications of DIC on concrete is in Choi and Shah,<sup>15</sup> where the compressive behavior is studied. Many research works are available since then for understanding the fracture properties of concrete,<sup>16,17</sup> but primarily it was used in experimental mechanics<sup>18,19</sup> to determine stress distribution through strain field. The process involves capturing images at regular intervals and comparing them with the reference/primary image, where the region of interest is split into multiple subsets. The images corresponding to the loaded stages of the structure are then compared to the primary image (in multiple subsets) to obtain surface displacements and thereby estimating the strain field distribution during the loading process.

The contribution of NSM CFRP reinforcement to the overall torsional behavior of thin walled tubular RC beams is assessed in this paper. Eight specimens (two reference and six strengthened beams) were tested experimentally to examine the performance of different strengthening configurations. DIC was used extensively to gain invaluable insights into the complex process of crack formation/propagation and to more accurately monitor CFRP strain evolution. DIC was also used to monitor the crack mouth opening displacements of the critical failure crack and of the other primary and secondary cracks.

## 2 | EXPERIMENTAL PROGRAMME

Eight beams were tested as part of this experimental programme, including two reference beams and six

strengthened beams using different NSM CFRP configurations. The strengthened beams were divided into two series: (a) Series 1 comprised four beams strengthened on all four faces, while (b) Series 2 comprised two beams strengthened only on three faces. The three-side strengthening configurations were investigated to examine the potential contribution of NSM FRP reinforcement in cases where access to all four faces is not possible, which is typical in many existing applications.

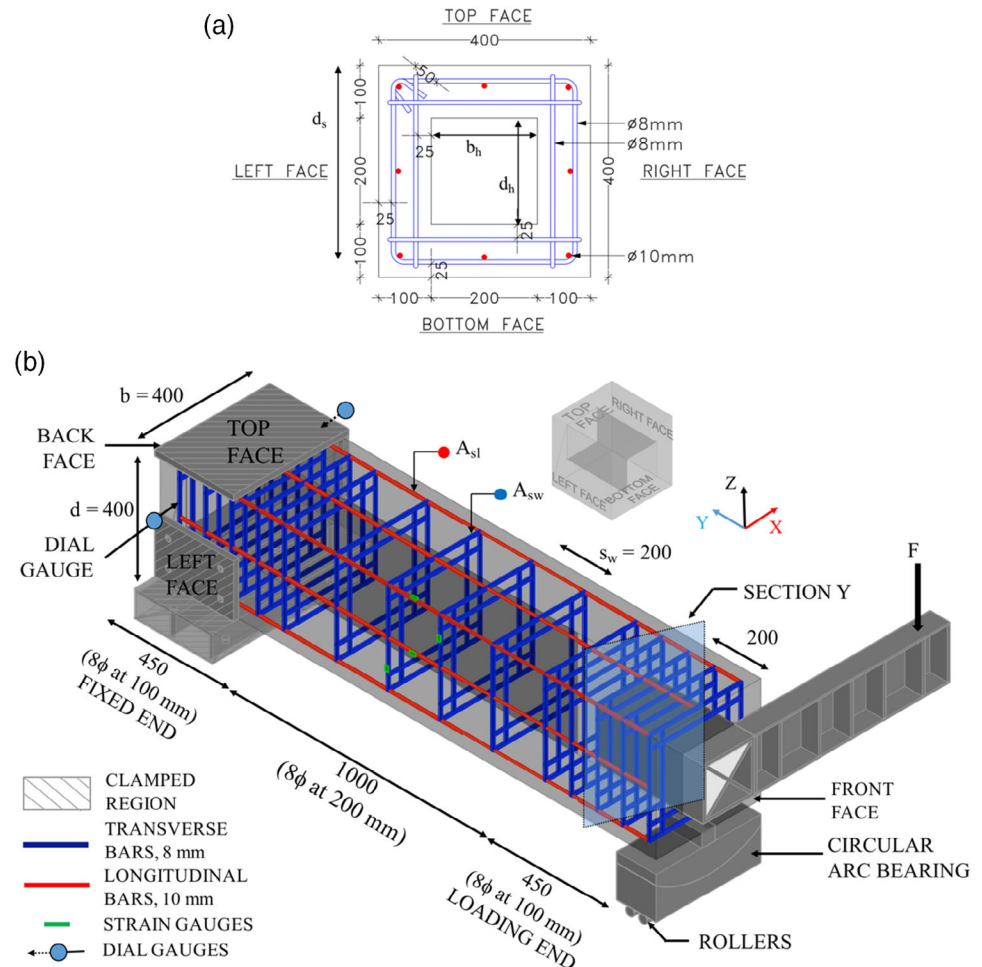
## 2.1 | Specimens

Figure 1 shows the cross sectional details of the tested beams, having a 400 mm × 400 mm outer cross section and an inner hollow section of 200 mm × 200 mm. Each beam has a total length of 1900 mm, with a central 1,000 mm long study area. The size of the specimens are designed to fail in torsion in the central study region (1,000 mm) of the beams, with wall thickness and reinforcement ratios representative of real applications in tubular type RC elements requiring torsional strengthening. Also, to attend the limitations of the test setup in terms of equipment, space

and reaction frame particularities. Finally it was conditioned by the financial resources available and the time period allowed to carry out the experimental program according to the funding research project. The longitudinal reinforcement consists of 8 bars with a diameter of 10 mm positioned in the four corners and in the center of each side. The transverse reinforcement consists of four-legged 8 mm diameter links, with 25 and 75 mm external and internal covers, respectively. In the central region, the stirrups are spaced at 200 mm centers, while the spacing is decreased to 100 mm in the end zones (450 mm from each end). The reduced spacing aims to prevent failure in the proximity of the loading and clamping areas of the beam during testing, the details of which are explained in Section 2.3. All beams in this experimental programme are manufactured with a C25/30 concrete.

### 2.1.1 | Material properties

The compressive strength and modulus of elasticity of the concrete at 28 days were obtained from tests on three and five concrete cylinders with an average diameter of



**FIGURE 1** Beam geometry. (a) Cross section. (b) Isometric section (all dimensions are in mm)

| Property                                   | $\phi 8$ (mm) | Co.V. (%) | $\phi 10$ (mm) | Co.V. (%) |
|--|---------------|-----------|----------------|-----------|
| Modulus of elasticity, $E_{sm}$ (GPa)      | 195.98        | 0.45      | 205.73         | 10.25     |
| Yield stress, $f_{ym}$ (MPa)               | 566.71        | 7.45      | 449.49         | 2.69      |
| Yield strain, $\epsilon_{ym}(\mu\epsilon)$ | 3.06          | 11.53     | 2.46           | 22.87     |
| Tensile strength, $f_{um}$ (MPa)           | 680.27        | 4.74      | 560.99         | 1.48      |

**TABLE 1** Properties of steel reinforcement

150 mm and height of 300 mm according to code specifications.<sup>20</sup> A mean compressive strength,  $f_{cm}$ , of 31.80 MPa (2.8%) and modulus of elasticity,  $E_{cm}$ , of 34.53 GPa (3.5%) were obtained, respectively (the values in parenthesis are the corresponding coefficient of variation). Five samples of 8 mm and 10 mm diameter bars were tested according to (EN\_10002-1 (1990)<sup>21</sup>) to determine their mean yield stress,  $f_{ym}$ , modulus of elasticity,  $E_{sm}$ , and ultimate strength,  $f_{um}$ . The results of the corresponding steel reinforcements are presented in Table 1. Tests on five samples from two different batches were carried out on the CFRP laminates to determine their tensile strength,  $f_{tu}$ , and modulus of elasticity,  $E_{fm}$ , according to (ISO<sup>22</sup>), and the results are presented in Table 2.

## 2.2 | Strengthening schemes

The strengthening configurations adopted in this research study are grouped into two categories: (a) four face strengthening and (b) three face strengthening using straight CFRP laminates as shown in Figure 2. It should be mentioned that the strengthening schemes in Series 1 requires clear access to all four faces. However, in real case scenarios it is usually difficult to access all four sides due to the presence of structural or non-structural elements. Hence, Series 2 strengthening configurations involve strengthening on three faces. The transverse laminates are spaced at 65 mm ( $s = (\frac{1}{3})200 = 65$ ) and 40 mm ( $s = (\frac{1}{5})200 = 40$ ), while the longitudinal laminates are spaced at 135 mm ( $s = (\frac{1}{3})400 = 135$ ) and 80 mm ( $s = (\frac{1}{5})400 = 80$ ). The transverse laminates are spaced such that the expected 45° spiral cracks are intersected by at least one (200 mm spacing) or two (100 mm spacing) laminates. The reinforcement ratios in both the longitudinal and transverse directions vary for each of the beams, tested as part of the two series. The reinforcement ratios are calculated according to Equations (1) and (2), using equivalent longitudinal ( $\rho_{l,eq}$ ) and transverse ( $\rho_{w,eq}$ ) reinforcement ratios.<sup>23</sup>

$$\rho_{l,eq} = \frac{A_{sl}}{(bd_s - b_h d_h)} + \left[ \frac{A_f E_f}{E_s} \frac{1}{(bd_f - b_h d_h)} \right] \quad (1)$$

$$\rho_{w,eq} = \frac{A_{sw}}{(b_w s_w)} + \left[ \frac{A_f E_f}{E_s} \frac{1}{(b_s d_f)} \right] \quad (2)$$

where  $A_{sl}$ ,  $b$  and  $d_s$  are, respectively, the cross sectional area, breadth and the internal arm of the existing longitudinal steel bars;  $A_f$  and  $d_f$  are the cross sectional area and the lever arm of the internal longitudinal CFRP;  $E_s$  and  $E_f$  are the modulus of elasticity of the steel and CFRP;  $b_w$  is the width of web (100 mm);  $b_h$  and  $d_h$  are the breadth and depth of the hollow section;  $A_{sw}$  and  $s_w$  are the cross sectional area and the spacing of the transverse reinforcement (Figure 2a). The values of these variables are indicated in Table 3.

The reference beams are named ‘‘Ref\_4S’’ and ‘‘Ref\_1S,’’ where ‘‘Ref’’ stands for reference and 4S and 1S represent the number of steel stirrups in the central monitoring zone. In the case of the strengthened beams, their designation is of the format ‘‘SxF\_LySz,’’ where ‘‘SxF’’ indicates the series strengthened (S) on four or three faces (‘‘x’’ equal to 4 or 3, respectively). The second term of the beam ID, ‘‘LySz,’’ is composed of ‘‘Ly’’ that indicates the number, y, of CFRP laminates on each face of the beam in the longitudinal direction, L, while ‘‘Sz’’ indicates the number, z, of CFRP laminates on each face of the beam in the transverse direction, S (stirrup). For example, ‘‘S4F\_L2S5’’ represents the beam of Series 1 (S4F, while S3F is Series 2), strengthened on four faces with two laminates in the longitudinal direction and five laminates in the transverse direction on each face of the beam.

The configurations adopted for the four-faces strengthened series (S4F) are shown in Figure 2a–d, while the configurations of the series of beams strengthened in three-faces (S3F) are shown in Figure 2e,f. A summary of all beam reinforcement details are given in Table 3 in terms of area of longitudinal steel ( $A_{sl}$ ), longitudinal steel reinforcement ratio ( $\rho_{sl}$ ), longitudinal CFRP strengthening ratio ( $\rho_{fl}$ ), area of transverse steel reinforcement ( $A_{sw}$ ), transverse steel reinforcement ratio ( $\rho_{sw}$ ), transverse CFRP strengthening ratio ( $\rho_{fw}$ ), spacing of the longitudinal CFRP laminates ( $s_{fl}$ ) and spacing of transverse CFRP laminates ( $s_{fw}$ ).

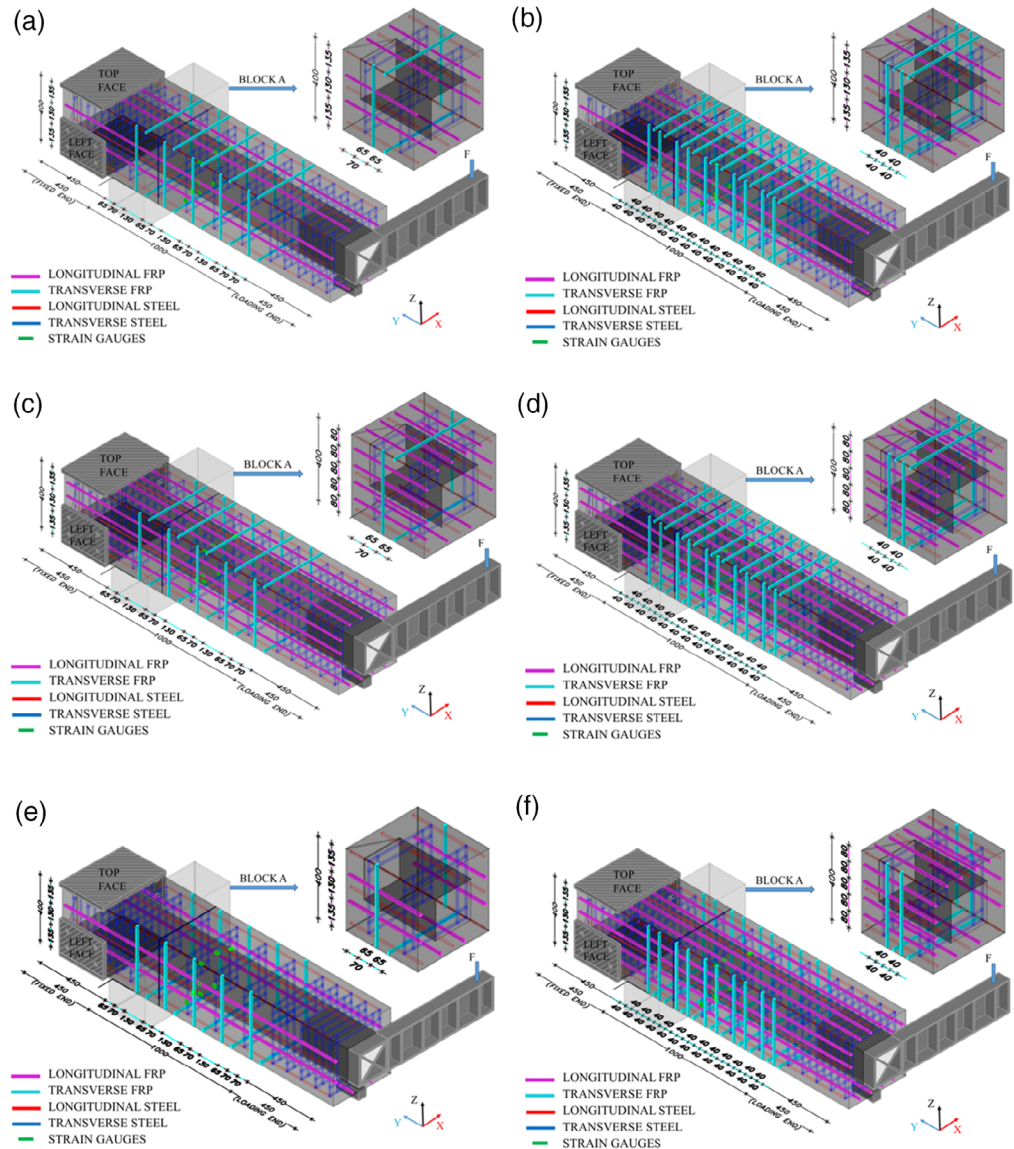
The CFRP laminates were manufactured by Clever reinforcement Iberica company. The laminates have a cross section of 10 mm  $\times$  1.4 mm. The first three

**TABLE 2** Properties of carbon fiber reinforced polymer (CFRP) laminates

| Property | Tensile strength, (MPa) $f_{um}$ | Co.V. (%) | Modulus of elasticity, $E_{fm}$ (GPa) | Co.V. (%) |
|----------|----------------------------------|-----------|---------------------------------------|-----------|
| Batch 1  | 2,346                            | 1.20      | 205.04                                | 5.60      |
| Batch 2  | 1982                             | 3.30      | 199.83                                | 1.40      |

**FIGURE 2**

Strengthening configurations:  
 (a) S4F\_L2S5, (b) S4F\_L2S10,  
 (c) S4F\_L4S5, (d) S4F\_L4S10,  
 (e) S3F\_L2S5, and (f)  
 S3F\_L4S10 (all dimensions  
 in mm)



beams of Series 1 (S4F\_L2S5, S4F\_L2S10, S4F\_L4S5) were strengthened with CFRP laminates from the same batch (Batch I), while beam S4F\_L4S10 and the two beams of Series 2 were strengthened with CFRP laminates from a different batch (Batch II) both in the longitudinal and transverse direction.

As part of the strengthening process, the longitudinal CFRP laminates were placed first, at a depth of 22 mm, followed by the transverse laminates at a depth of 12 mm. The grooves in the RC beam were cut at the designated locations and with the required dimensions using

a laser-guided tool. The selected groove depths are smaller than the ACI (440.2R-08<sup>24</sup>) guidelines due to the limited concrete cover, representing real case scenario. After the grooves were cut, the strengthening process involved the following steps:

- The grooves are cleaned with air pressure;
- The CFRP laminates are cleaned with acetone to remove any dust particles;
- The epoxy is prepared according to the prescribed hardener to resin ratio (1:4);

**TABLE 3** Reinforcement and strengthening ratios, and spacing of carbon fiber reinforced polymer laminates in Series 1 (S4F) and 2 (S3F) of strengthened beams

| Beam                       | $A_{sl}$ (mm <sup>2</sup> ) | $\rho_{sl}$ (%) | $\rho_{fl}$ (%) | $\rho_{l,eq}$ (%) | $A_{sw}$ (mm <sup>2</sup> ) | $\rho_{sw}$ (%) | $\rho_{fw}$ (%) | $\rho_{w,eq}$ (%) | $s_{fl}$ (mm) | $s_{fw}$ (mm) |
|----------------------------|-----------------------------|-----------------|-----------------|-------------------|-----------------------------|-----------------|-----------------|-------------------|---------------|---------------|
| S4F_L2S5<br>(Figure 3a)    | 628                         | 0.571           | 0.096           | 0.667             | 50.24                       | 0.502           | 0.071           | 0.573             | 134           | 65            |
| S4F_L2S10<br>(Figure 3b)   | 628                         | 0.571           | 0.096           | 0.667             | 50.24                       | 0.502           | 0.141           | 0.644             | 134           | 40            |
| S4F_L4S5<br>(Figure 3c)    | 628                         | 0.571           | 0.192           | 0.763             | 50.24                       | 0.502           | 0.071           | 0.573             | 80            | 65            |
| S4F_L4S10<br>(Figure 3d)   | 628                         | 0.571           | 0.192           | 0.763             | 50.24                       | 0.502           | 0.141           | 0.644             | 80            | 40            |
| S3F_L2S5<br>(Figure 3e)    | 628                         | 0.571           | 0.072           | 0.643             | 50.24                       | 0.502           | 0.053           | 0.555             | 135           | 65            |
| S3F_L4S10<br>(Figure 3(f)) | 628                         | 0.571           | 0.144           | 0.715             | 50.24                       | 0.502           | 0.106           | 0.608             | 80            | 40            |

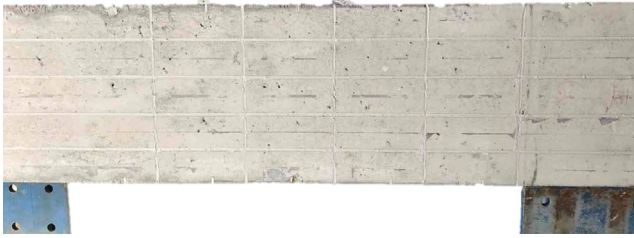


**FIGURE 3** Appearance of a strengthened face of the S4F\_L4S5 beam

- The grooves are filled with epoxy and a layer of epoxy is also applied on the two large faces of the CFRP laminates;
- The CFRP laminates are inserted into the grooves, and the excess epoxy is removed from the surface of the beam;
- The beam is set to dry for a week, even though the recommended minimum curing time is only 2 days.

Figure 3 shows one of the faces of the S 4F\_L4S5 beam after has been strengthened.

## 2.3 | Test setup

The test setup adopted for all experimental tests is shown in Figure 4a. The boundary conditions consist of a loading end and a fixed end. The fixed end comprises a steel frame and a hydraulic jack in between an element of this frame and the bottom surface of the beam to adjust the height of the beam and firmly fix it, thus restricting all translations and rotations. The loading end of the beam consisted of a steel loading section connected to a load cell through multiple hinges to minimize the

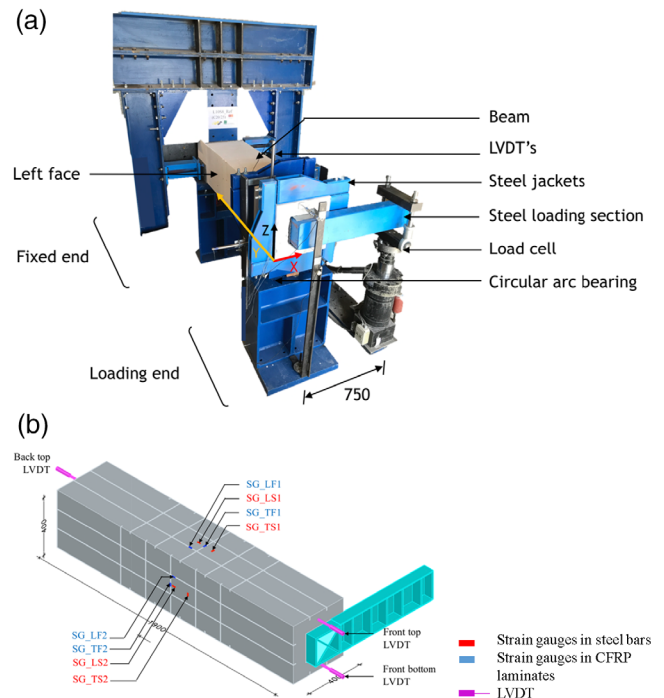


**FIGURE 4** (a) Test setup, and (b) location of LVDT's

development of any additional eccentric force during the test. Load is applied through a L-type steel loading section, where one end of this section is inserted inside the hollow section of the beam (up to 300 mm) and the other end is connected to load cell through multiple hinges to apply the load, converting it into moment. The beam was rested on a pinned support, which was placed on a circular arc bearing (CAB) with a rotational arc radius of 350 mm from the center of the beam. Rollers were also placed below the CAB to accommodate any elongation or shortening of the beam during testing. More details on the test setup can be found in.<sup>23</sup> Two steel jackets were

placed in the over-reinforced region of the beam loading end in an attempt to avoid the premature failure in this region. The development of this test setup was assisted by performing comprehensive numerical analysis, complemented with parametric studies for assessing the influence of different strengthening configurations and material properties on the torsional strengthening effectiveness.<sup>25</sup>

The experimental tests were performed under displacement control at a loading rate of 1.2 mm/min. Linear Variable Differential Transformers (LVDTs) were placed on all the faces in the loading end to measure the average torsional angle of rotation. Additional LVDTs were also positioned along the front and back face of the beam to measure relative elongation or shortening. An inclinometer was also applied inside the hollow section to measure the angle of rotation. Dial gauges were placed on the extreme right and left faces at the fixed end to measure any translations that could take place during testing.

A 2D DIC setup was used on the left face of each beam to monitor the distribution of deformations along the central study zone of 1,000 mm, in order to obtain detailed information on the crack initiation and propagation, for better interpretation of the resisting mechanisms in this loading stage. Due to the available testing space limitations, and considering the main purpose of qualitatively assessing the cracking process in a representative beam's face, the option was to use a single camera with an optimized positioning in order to capture the entire testing area of one of the beam's faces. Therefore, only in-plane displacements and deformations were traced, considering the plane of the imaged face of the beam. A 24 mm by 36 mm complementary metal-oxide semiconductor (CMOS) sensor, with a resolution of approximately 36 megapixels, was used. The objective lens adopted had a focal distance of 44 mm and the aperture of  $f/11$ . Images were taken at a time interval of 10 s. The camera was mounted on a tripod at a distance of 1.22 m from the concrete surface. Two LED lights were used to ensure uniform light conditions during the tests. A speckle pattern was created on the surface using a very thin spray of black acrylic spray paint over an initial white spray.

## 3 | RESULTS

### 3.1 | General behavior: Series 1 and Series 2

#### 3.1.1 | Torsional moment versus torsional angle of rotation

Figure 5a shows the torsional moment versus torsional angle of rotation for the reference and strengthened

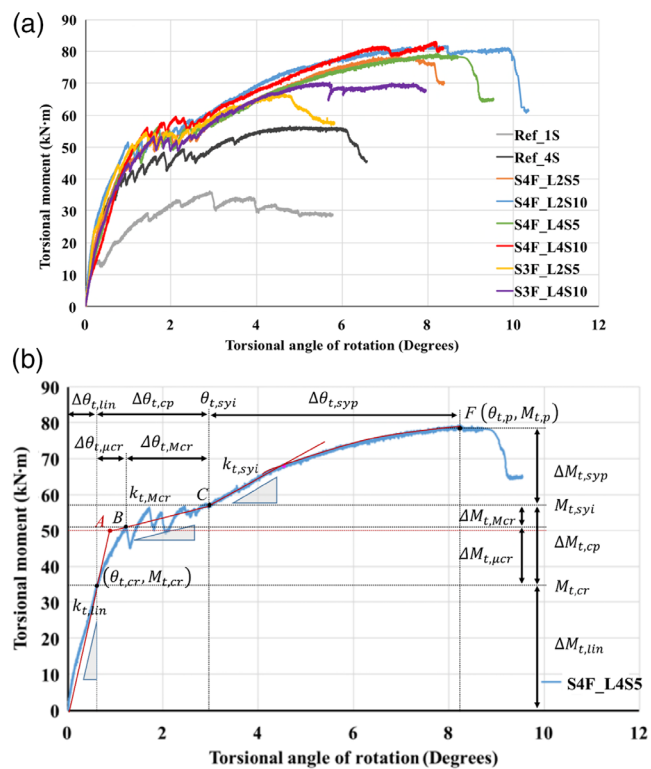


**FIGURE 5** (a) Torsional moment versus torsional angle of rotation (b) General behavior of near surface mounted (NSM) strengthened beams

beams of both series (S4F and S3F). Figure 5b shows the typical behavior of a strengthened beam, while Tables 4–6, summarize the experimental values for all tested beams in terms of torsional moment, torsional angle of rotation and stiffness at cracking moment, yield initiation and peak moment. The main observations from the tests are summarized in the following, while a more detailed account of the performance of each of the tested beams is given in References 23 and 26.

The general torsional response of the strengthened beams is characterized by three distinct phases: (a) linear elastic; (b) crack propagation; and (c) post-yielding of steel reinforcement.

1. Linear elastic phase: from the initiation of the test up to the torsional cracking moment ( $\theta_{t,cr}$ ,  $M_{t,cr}$ ). The performance of the beam is primarily governed by the concrete response, while the reinforcement contribution is almost negligible.
2. Crack propagation phase: from the torsional cracking moment up to a load level at which the process of crack formation stabilizes, considered to be coinciding with yielding of the steel reinforcement. This phase can further be divided into two sub-phases: (a) micro-cracking phase where many cracks initiate following

**TABLE 4** Experimental results of tested beams in terms of torsional moment

| Beam                    | $M_{t,cr}$ (kN·m) | $\left(\frac{M_{t,cr}^S - M_{t,cr}^R}{M_{t,cr}^R}\right)$ | $M_{t,Mcr}$ (kN·m) | $M_{t,sysi}$ (kN·m) | $\left(\frac{M_{t,sysi}^S - M_{t,sysi}^R}{M_{t,sysi}^R}\right)$ | $M_{t,p}$ (kN·m) | $\left(\frac{M_{t,p}^S - M_{t,p}^R}{M_{t,p}^R}\right)$ |
|-------------------------|-------------------|---|--------------------|---------------------|---|------------------|--|
| Ref_4S<br>(Series 1)    | 28.01             | -   | 41.44              | 47.29               | -   | 56.69            | -  |
| S4F_L2S5                | 25.04             | -10.61  | 44.43              | 55.23               | 16.79   | 78.30            | 38.11  |
| S4F_L2S10               | 28.46             | 1.64  | 51.17              | 57.63               | 21.87   | 81.69            | 44.09  |
| S4F_L4S5                | 34.41             | 22.87   | 50.40              | 56.40               | 19.27   | 79.37            | 39.99  |
| S4F_L4S10               | 39.26             | 40.17   | 55.51              | 59.39               | 25.58   | 83.02            | 46.43  |
| Average                 | 31.79             |   | 50.38              | 57.16               |   | 80.59            |  |
| Co.V. (%)<br>(Series 2) | 19.84             |   | 9.05               | 3.11                |   | 2.67             |  |
| S3F_L2S5                | 23.69             | -15.43  | 44.00              | 56.28               | 19.02   | 66.65            | 17.57  |
| S3F_L4S10               | 26.57             | -5.14   | 44.78              | 55.57               | 17.51   | 70.27            | 23.94  |
| Average                 | 25.13             |   | 44.39              | 55.92               |   | 68.46            |  |
| Co.V. (%)               | 8.11              |   | 1.24               | 0.90                |   | 3.43             |  |

Note:  $M_{t,cr}^{S/R}$ : S and R stand for, respectively, strengthened and reference beam.

**TABLE 5** Experimental results of tested beams in terms of angle of rotation

| Beam                    | $\theta_{t,cr}$ (deg) | $\left(\frac{\theta_{t,cr}^S - \theta_{t,cr}^R}{\theta_{t,cr}^R}\right)$ | $\theta_{t,Mcr}$ (deg) | $\theta_{t,sysi}$ (deg) | $\left(\frac{\theta_{t,sysi}^S - \theta_{t,sysi}^R}{\theta_{t,sysi}^R}\right)$ | $\theta_{t,p}$ (deg) | $\left(\frac{\theta_{t,p}^S - \theta_{t,p}^R}{\theta_{t,p}^R}\right)$ | $\mu_{t,y} = \frac{\theta_{t,p}}{\theta_{t,cr}}$ | $\mu_{t,cr} = \frac{\theta_{t,p}}{\theta_{t,cr}}$ |
|-------------------------|-----------------------|--|------------------------|-------------------------|--|----------------------|---|--|---|
| Ref_4S<br>(Series 1)    | 0.39                  | -  | 0.93                   | 2.77                    | -  | 4.78                 | -   | 1.73   | 12.32   |
| S4F_L2S5                | 0.33                  | -14.43   | 0.88                   | 2.76                    | -0.44  | 7.31                 | 53.01   | 2.65   | 22.03   |
| S4F_L2S10               | 0.30                  | -23.20   | 0.99                   | 2.57                    | -7.24  | 8.40                 | 75.83   | 3.27   | 28.20   |
| S4F_L4S5                | 0.62                  | 59.28  | 1.19                   | 2.94                    | 5.97   | 8.23                 | 72.21   | 2.80   | 13.32   |
| S4F_L4S10               | 0.78                  | 101.88   | 1.45                   | 2.97                    | 7.22   | 8.19                 | 71.43   | 2.76   | 10.46   |
| Average                 | 0.51                  |  | 1.13                   | 2.81                    |  | 8.04                 |   | 2.87   | 18.50   |
| Co.V. (%)<br>(Series 2) | 45.90                 |  | 21.97                  | 6.56                    |  | 6.10                 |   | 9.54   | 43.91   |
| S3F_L2S5                | 0.21                  | -45.62   | 0.75                   | 2.70                    | -2.39  | 4.63                 | -3.17   | 1.71   | 21.93   |
| S3F_L4S10               | 0.44                  | 13.85  | 1.02                   | 2.78                    | 0.48   | 5.71                 | 19.48   | 2.05   | 12.93   |
| Average                 | 0.33                  |  | 0.89                   | 2.74                    |  | 5.17                 |   | 1.88   | 17.43   |
| Co.V. (%)               | 0.50                  |  | 21.28                  | 2.05                    |  | 14.81                |   | 12.77  | 36.53   |

Note:  $\theta_{t,cr}^{S/R}$ : S and R stand for, respectively, strengthened and reference beam.

the development of the torsional cracking moment; (b) macro-cracking phase where major cracks form on all the faces of the beam. The relative loss in torsional resistance decreases with the increase in applied torsional angle until no new torsional cracks develop. The stiffness associated with this phase, that is, the stiffness at stabilized cracking, is determined as ( $k_{t, Mcr} = \Delta M_{t, Mcr} / \Delta \theta_{t, Mcr}$ ) and represents the slope of the line connecting the peak before the first major drop after the torsional cracking moment, and the first point identified as the yielding of the reinforcement. During this phase, both the steel reinforcement and

CFRP reinforcement contribute to the overall torsional resistance.

3. Post-yielding of steel reinforcement: from the initiation of steel yielding ( $\theta_{t,sysi}$ ,  $M_{t,sysi}$ ) to the peak torsional moment ( $\theta_{t,p}$ ,  $M_{t,p}$ ). Most of the steel reinforcement develops some degree of yielding before the peak torsional moment is reached. As the response of this phase follows a non-linear ductile behavior, the stiffness ( $k_{t,sysi}$ ) is measured only in its initial stage. During this last phase, the contribution of steel reinforcement can be considered to be constant while the torsional resistance offered by the



**TABLE 6** Experimental results of the tested beams in terms of torsional stiffness

| Beam                    | $k_{t,lin}$ (kN·m/deg) | $\left(\frac{k_{t,lin}^S - k_{t,lin}^R}{k_{t,lin}^R}\right)$ | $k_{t,Mcr}$ (kN·m/deg) | $\left(\frac{k_{t,Mcr}^S - k_{t,Mcr}^R}{k_{t,Mcr}^R}\right)$ | $k_{t,sysi}$ (kN·m/deg) | $\left(\frac{k_{t,sysi}^S - k_{t,sysi}^R}{k_{t,sysi}^R}\right)$ |
|-------------------------|------------------------|--|------------------------|--|-------------------------|---|
| Ref_4S<br>(Series 1)    | 69.80                  | -  | 4.02                   | -  | 7.36                    | -   |
| S4F_L2S5                | 64.46                  | -7.66  | 5.77                   | 43.64  | 6.10                    | -17.06  |
| S4F_L2S10               | 87.30                  | 25.07  | 5.97                   | 48.60  | 7.69                    | 4.58  |
| S4F_L4S5                | 45.08                  | -35.41   | 3.74                   | -7.03  | 7.49                    | 1.81  |
| S4F_L4S10               | 48.43                  | -30.61   | 3.42                   | -14.84   | 6.20                    | -15.76  |
| Average                 | 61.32                  |  | 4.73                   |  | 6.87                    |   |
| Co.V. (%)<br>(Series 2) | 31.43                  |  | 28.20                  |  | 12.19                   |   |
| S3F_L2S5                | 68.91                  | -1.28  | 4.88                   | 21.52  | 7.44                    | 1.12  |
| S3F_L4S10               | 66.81                  | -4.28  | 4.48                   | 11.41  | 9.88                    | 34.30   |
| Average                 | 67.86                  |  | 4.68                   |  | 8.66                    |   |
| Co.V. (%)               | 2.19                   |  | 6.14                   |  | 19.93                   |   |

Note:  $k_{t,cr}^{S/R}$ : S and R stand for, respectively, strengthened and reference beam.

CFRP laminates further increases until failure of the beam is reached.

The linear torsional stiffness of the beams strengthened on three and four faces, except S4F\_L2S10 beam, have decreased with respect to the reference beam. However, in case of three face strengthened beams, the stiffness is very close to the reference beam. In terms of torsional cracking moment,  $M_{t,cr}$ , beams strengthened on all four faces with four longitudinal laminates exhibit the maximum increase (31.52% average), whereas a reduction in performance is registered in all other beams, irrespective of the adopted strengthening scheme. Similarly, in terms of angle at torsional cracking moment, Series 1 beams with the four faces strengthened with four longitudinal CFRP laminates have registered an average increase of 80.58%, while all other beams, except S3F\_L2S5, have presented smaller  $\theta_{t,cr}$ . This variation in torsional cracking moment and angle of rotation at cracking moment can be attributed to normal variability of material properties, beam geometry and stiffness at the supports. It should be noted, however, that the determination of both  $M_{t,cr}$  and  $\theta_{t,cr}$  is highly susceptible and dependent on the accurate detection of crack initiation by visual inspection of all the four faces of the beams.

All beams, with the exception of S4F\_L4S5 and S4F\_L4S10, exhibit a higher torsional stiffness at macro cracking, with respect to the reference beam due to the contribution of the CFRP laminates in resisting torsion. Higher values of torsional moment at yield initiation,  $M_{t,sysi}$ , also developed in all strengthened beams. Beams strengthened with the highest amount of transverse reinforcement exhibit

an overall better performance than the beams strengthened with lower amounts of CFRP transverse reinforcement. The angle of rotation at yield initiation of all strengthened beams does not seem to be affected by the presence of the CFRP strengthening reinforcement.

The torsional stiffness at yield initiation,  $k_{t,sysi}$ , has decreased in S4F\_L2S5 and S4F\_L4S10, and beam S3F\_L4S10 has presented the highest increase. The rest of the beams have shown negligible increase between 1 and 5%. In terms of torsional moment at peak and its corresponding angle of rotation,  $M_{t,p}$  and  $\theta_{t,p}$ , respectively, all of the strengthened beams have enhanced performance with respect to the reference beam, due to the effective contribution of the CFRP laminates, being visible the favorable contribution of the transverse CFRP reinforcement in this regard.

### 3.1.2 | Crack spacing and failure modes

Table 7 presents the experimentally determined values of crack spacing and crack orientation. The crack spacing,  $s_{rm}$ , is calculated as the average distance between fully developed cracks on all four faces of a beam. Similarly, the angle of inclination,  $\alpha_{crm}$ , is measured as an average orientation of all the cracks evaluated with respect to the longitudinal axis of the beam. All strengthened beams have shown a reduction of crack spacing, varying between 16 and 49% with respect to the reference beam. Beams strengthened with the highest transverse CFRP reinforcement ratio have shown the maximum reduction in spacing, by an average of 43%, that is, the spacing between

**TABLE 7** Average crack spacing ( $s_{rm}$ ) and crack orientation ( $\alpha_{crm}$ ) of the tested beams

| Beam      | Average crack spacing<br>$s_{rm}$ (mm) | $\left(\frac{s_{rm}^S - s_{rm}^{R,4S}}{s_{rm}^{R,4S}}\right) 100$ (%) | Average crack orientation,<br>$\alpha_{crm}$ (degrees) |
|-----------|--|---|--|
| Ref_1S    | 417.92                                 | -   | 49.61  |
| Ref_4S    | 200.28                                 | -   | 50.09  |
| S4F_L2S5  | 132.59                                 | -33.80  | 51.34  |
| S4F_L2S10 | 104.48                                 | -47.83  | 53.70  |
| S4F_L4S5  | 133.33                                 | -33.43  | 49.13  |
| S4F_L4S10 | 101.37                                 | -49.38  | 49.32  |
| S3F_L2S5  | 169.20                                 | -15.52  | 49.33  |
| S3F_L4S10 | 139.90                                 | -30.15  | 50.83  |

Note:  $s_{rm}^{S/R,4S}$ : S and R stand for strengthened and reference beam, respectively.

cracks decreased from 200 mm (Ref\_4S) to an average of 115 mm. The transverse CFRP laminates are effective in reducing crack spacing, arresting the crack growth, and thereby increasing the torsional moment carrying capacity of the beams due to a more effective mobilization of the aggregate interlock shear resisting mechanism (Table 4).

Figure 6 shows the failure modes of all tested beams. In Series 1, beams S4F\_L2S5, S4F\_L2S10 and S4F\_L4S5 failed by CFRP rupture followed by concrete crushing, while beam S4F\_L4S10 failed by premature concrete failure in the over-reinforced region due to stress concentration around the steel loading section. In Series 2, beam S3F\_L2S5 failed by concrete crushing on the unstrengthened top surface, while beam S3F\_L4S10 has prematurely failed, similarly to beam S4F\_L4S10.

### 3.1.3 | Ductility performance of strengthened beams

The increased torsional moment carrying capacity of the strengthened beams is evident through previous section. In order to further evaluate the strengthening efficiency, two ductility index ratios are introduced to quantify the ductility performance of beams strengthened with NSM CFRP laminates in torsion.<sup>27</sup> These ratios are calculated according to the Equations (3) and (4) presented below:

$$\mu_{t,y} = \frac{\theta_{t,p}}{\theta_{t,sy}} \quad (3)$$

$$\mu_{t,cr} = \frac{\theta_{t,p}}{\theta_{t,cr}} \quad (4)$$

where  $\theta_{t,p}$ , indicates the peak torsional angle of rotation,  $M_{t,p}$  and  $M_{t,cr}$  indicates the ductility performance of beams with respect to peak torsional moment and torsional cracking moment. The corresponding values of each beam is presented in Table 5. Based on the results, it is evident the contribution of NSM CFRP laminates in increasing the ductility performance of the beams in Series 1 by 114 and by 15% in Series 2 with respect to angle of rotation at yielding point, and by 618% in Series 1 and by 511% in Series 2 with respect to angle of rotation at cracking moment.

## 3.2 | Digital image correlation

### 3.2.1 | General response of strengthened beams

The central study zone of the left face of both reference and strengthened beams was monitored with 2D-DIC to examine in detail the influence of the investigated strengthening solutions on the overall deformation behavior. Typical crack evolution and global behavior are described using strengthened beam S4F\_L4S5 and reference beam Ref\_4S, followed by a discussion on the effect of the various strengthening schemes. The crack development is presented in Figure 8, while the corresponding strain evolution in the CFRP reinforcement is presented in Figure 9. The longitudinal and transverse CFRP laminates are represented by white dotted lines, and the transverse and longitudinal steel reinforcement by yellow dotted lines in Figure 8. Full field major principal strain maps (tension) have been computed and represented for a strain range varying between 0 and 0.1. Although the strain maps computed are based on the assumption of continuous displacement fields, strong strain gradients may be seen as approximate representations of discrete displacements such as cracks, provided that the resolution of the system is sufficiently high. While the overall deformation behavior is similar for all strengthened beams, the magnitude of the strain field at failure is mainly affected by the amount of CFRP laminates forming the strengthening system. The observed crack types (Figure 7) can be categorized as follows:

1. Primary cracks (Type I): parallel spiral cracks extending throughout the whole length of the beam;
2. Secondary cracks (Type II): new individual cracks (Type IIa) or originating from existing primary cracks (Type IIb) only extending along one side of the beam and with typical length of ~200 mm and more;
3. Tertiary cracks: new individual cracks (Type IIIa) or originating from existing primary or secondary cracks

**FIGURE 6** Failure modes of the strengthened beams:  
 (a) S4F\_L2S5, (b) S4F\_L2S10,  
 (c) S4F\_L4S5, (d) S4F\_L4S10,  
 (e) S3F\_L2S5 and (f) S3\_L2S10

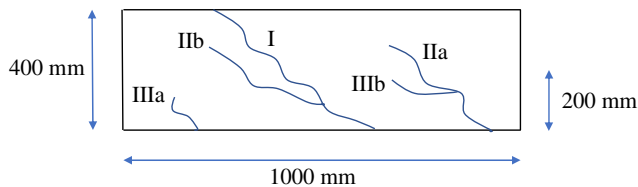
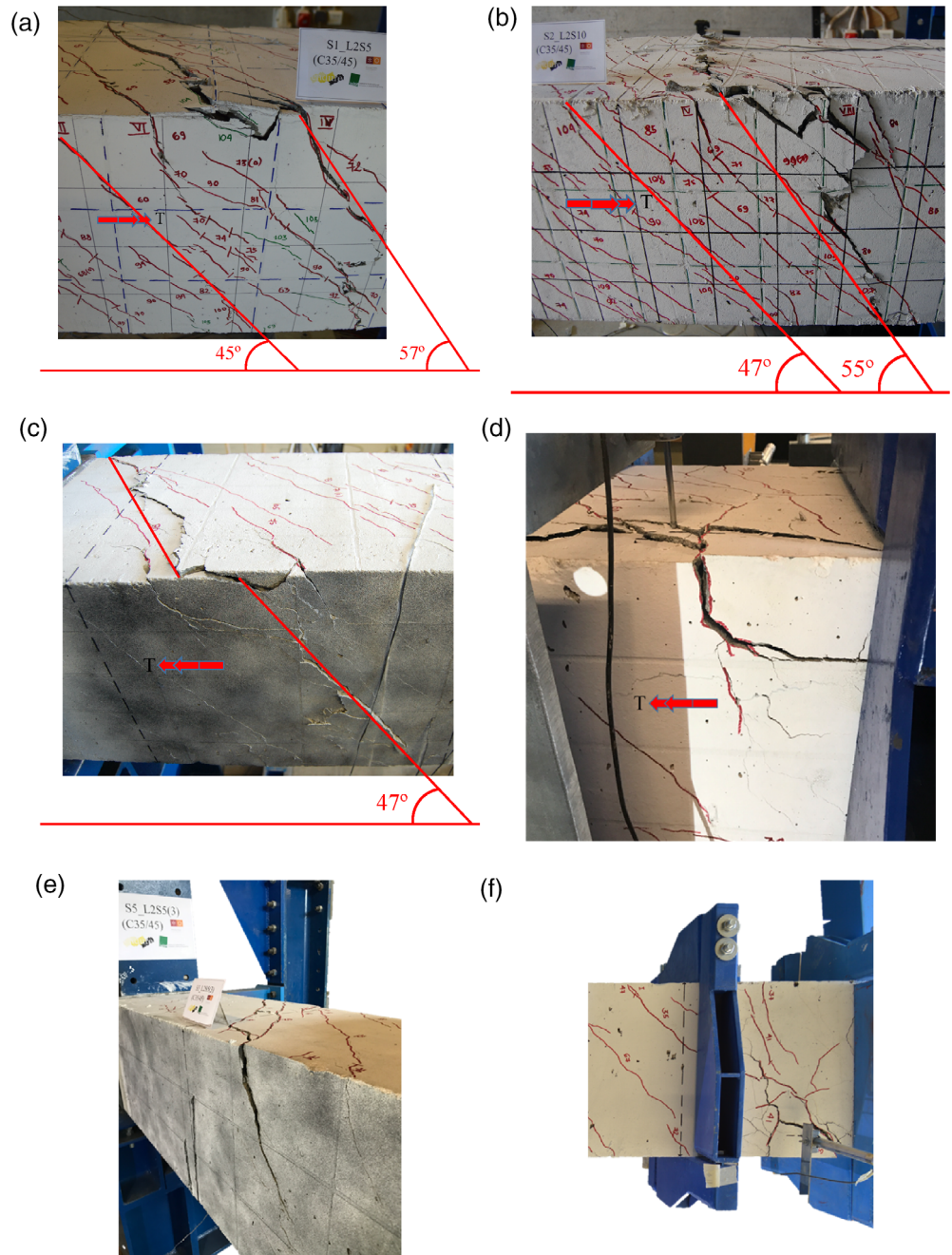


**FIGURE 7** Schematic representation of cracks

(Type IIIb) only extending along one side of the beam and with typical length smaller than 200 mm.

Cracking initiated with the formation of secondary (IIa) and tertiary cracks (IIIa) within the loading and

fixed end regions and subsequently extended into the central study region at an applied rotation and moment equal to 1.89° and 54.11 kN-m, respectively (Figure 8b). In the specimens with fully functioning internal strain gauges, crack initiation was also recorded by the strain gauges attached to the transverse steel reinforcement. At this stage, the beam enters in the macro/micro crack propagation phase, during which the initiation of new cracks, or the propagation of existing ones, is mainly observed within the central region. Although the contribution of concrete through aggregate interlock is still very significant, the moment carrying capacity is mainly guaranteed by the internal reinforcement and the NSM

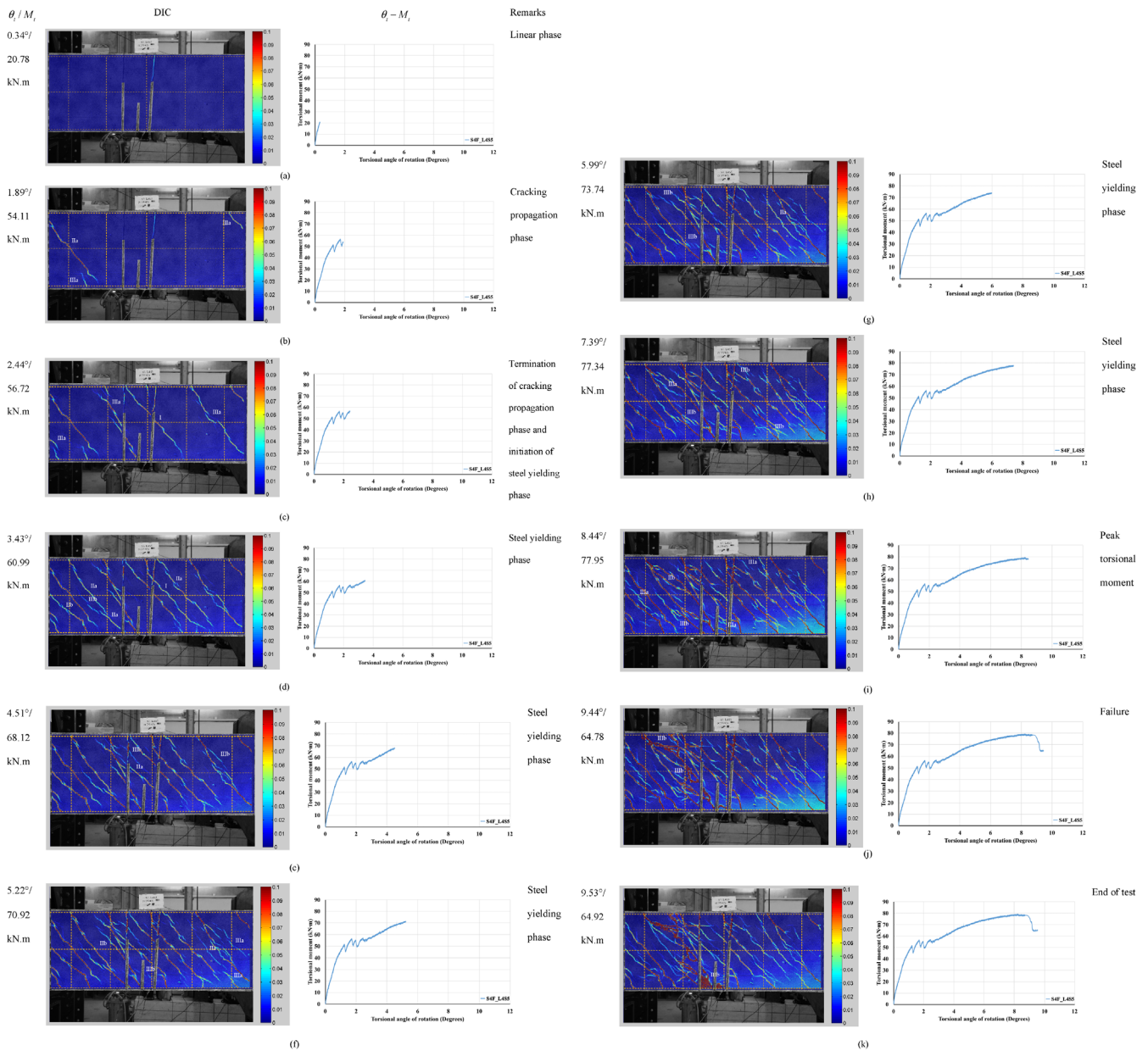


FIGURE 8 Cracking evolution of beam S4F\_L4S5 captured by digital image correlation (DIC)

CFRP, as evidenced by the increase in the recorded strains (Figure 9).

At 2.44° and 56.72 kN·m (Figure 8c), a primary crack formed in the middle of the beam along with a few tertiary cracks, which subsequently interconnected to form secondary and primary cracks. At this stage, the external transverse reinforcement started to contribute in resisting the torsional load and a sudden increase in the strain developed in the CFRP was observed (Figure 9: point “c”). Unfortunately, strain data for the internal steel reinforcement are not available as all of the strain gauges stopped functioning. As the applied torsional rotation increased, both the longitudinal and transverse CFRP laminates were successful at controlling the development

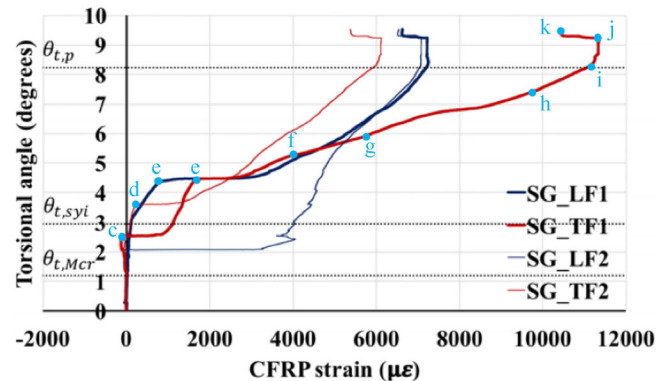


FIGURE 9 Carbon fiber reinforced polymer (CFRP) strain versus torsional angle of rotation of beam S4F\_L4S5

of primary cracks and mainly secondary and tertiary cracks formed after this stage. As a result, the presence of the external CFRP reinforcement contributed to the larger torsional deformability of the strengthened beams, increasing their ductility performance and torsional moment carrying capacity.

Crack stabilization and yielding of the steel reinforcement occurred at a value of applied torsional rotation and moment equal to  $2.94^\circ$  and  $56.40$  kN·m, respectively ( $\theta_{t, syi}$  and  $M_{t, syi}$  in Figure 9). The formation of new cracks, as well as the widening and interlinking of existing tertiary and secondary cracks, occurred at a lower rate after this stage, as shown in Figure 8d–f at  $3.43^\circ$ ,  $4.51^\circ$  and  $5.22^\circ$  with  $60.99$ ,  $68.12$  and  $70.92$  kN·m. The corresponding CFRP strain values are presented in Figure 9, points d, e and f. In the case of the reference beam, a sudden increase in steel strains between  $4,000$  and  $6,000$  micro strain is observed, whereas in the case of the strengthened beams, the strain in the steel reinforcement is limited to  $2000$  micro strain, since the torsional moment carrying capacity is distributed between the steel and the CFRP laminates.

With the further increase in the applied torsional moment, interlinking of existing cracks, between all three types of cracks took place at  $5.99^\circ$  and  $7.39^\circ$  with  $73.74$  and  $77.34$  kN·m (Figure 8g,h). At this stage the CFRP laminates were fully engaged in resisting the imposed torsional rotation. This is confirmed by the variation in the strain recorded along the CFRP laminates (Figure 9 points c–j). The crack pattern at peak torsional moment is shown in Figure 8i ( $8.44^\circ$ ,  $77.95$  kN·m and point “i” in Figure 9), quickly followed by the formation of primary cracks, softening of the torsional response and failure of the beam ( $9.44^\circ$ ,  $64.78$  kN·m). It can be observed from Figure 8d–k that the longitudinal and the transverse CFRP laminates controlled the crack growth, enhanced the aggregate interlock and promoted the formation of many secondary and tertiary cracks rather than the full development of primary cracks (cracks running full depth of the beam's cross section,  $400$  mm).

It can be concluded that the CFRP laminates in the initial stages successfully controlled the formation of primary cracks, and promoted the development of tertiary cracks (Figure 8c, IIIa) and secondary cracks (Figure 8i, IIb). However, at higher angle of rotation, closer to the peak moment, interconnection of tertiary and secondary cracks took place forming primary cracks, leading to failure (Figure 8j). Similarly, the evolution of crack pattern for beam S3F\_L2S5 (three face strengthened beam) follows the same procedure and is presented in Appendix A.

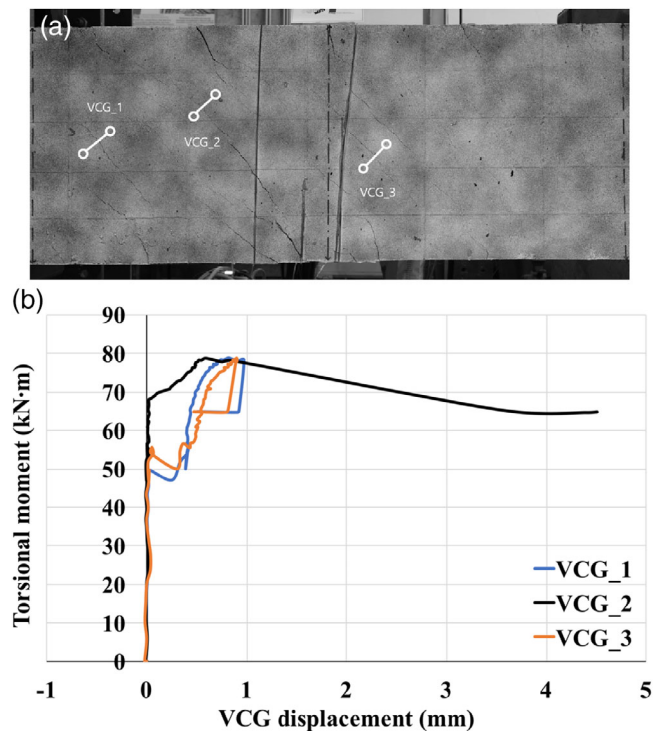


**FIGURE 10** (a) Location of virtual clip gauges (VCG) using digital image correlation (DIC), and (b) Torsional moment versus VCG deformation

### 3.2.2 | Crack mouth opening displacements

In order to further clarify the stiffening mechanisms occurred during crack initiation and propagation, the evolution of crack opening was derived at three specific locations for three cracks of S4F\_L4S5 beam. For the purpose, three virtual clip gauges (VCG) were created in the DIC procedure, by tracing the displacement in three pairs of points placed in opposite positions relative to a given crack. The position of the three VCG adopted is presented in Figure 10a. The displacement difference between the two points forming a VCG was then calculated in the direction which is approximately perpendicular to the crack plane. The VCG\_2 is located in the critical failure crack. The displacements obtained, which can be considered as an approximation of the opening of the corresponding crack projected to the plane of measurement (plane of the surface of the beam), are represented in Figure 10b.

As shown in Figure 10b, the crack monitored by VCG\_1 was the first one to develop. A sudden displacement increment was registered when the crack formed, and subsequently crack opening increased at a very low rate. A second crack, the opening of which was registered by VCG\_3, showed a sudden increase in width, similarly

to the previous crack represented by VCG\_1. The third crack to form, which was captured by VCG\_2, showed an even slower increase in width. This is most likely the result of the fact that, while the rotation imposed to the specimen was increasing and also the number of open cracks increased, the torsional stiffness decreased. Therefore, the suddenly imposed displacement increment that results from the opening of a new crack leads to a load drop that tends to be smaller. Additionally, it is also possible to observe that the cracks formed at later stages tend to show a more rapid subsequent increment of crack opening, probably due to the gradual deterioration of the bond conditions of the reinforcements. Lastly, all three cracks have reached approximately similar value of crack opening at peak moment (0.8 mm), at which point one of these developed in the critical failure crack (captured by VCG\_2).

### 3.2.3 | Reference beam: Ref\_4S

In the current section, the behavior of the reference beam “Ref\_4S” is described using DIC. The development of the cracks with respect to the increase in the applied torsional moment (vs. torsional angle of rotation) is presented in Figure 11, and the respective steel strain evolution is presented in Figure 12. The steel reinforcements, both the longitudinal and the transverse reinforcements are presented by yellow dotted lines in Figure 11.

In Figure 11a, the reference beam is in the linear response stage where no cracks are developed. The torsional cracking moment takes place in Figure 11b, where the first secondary crack is formed closer to the front loading region of the beam, at 0.49° and 30.87 kN·m. No steel strain jump is registered in any of the steel strain gauges, since the

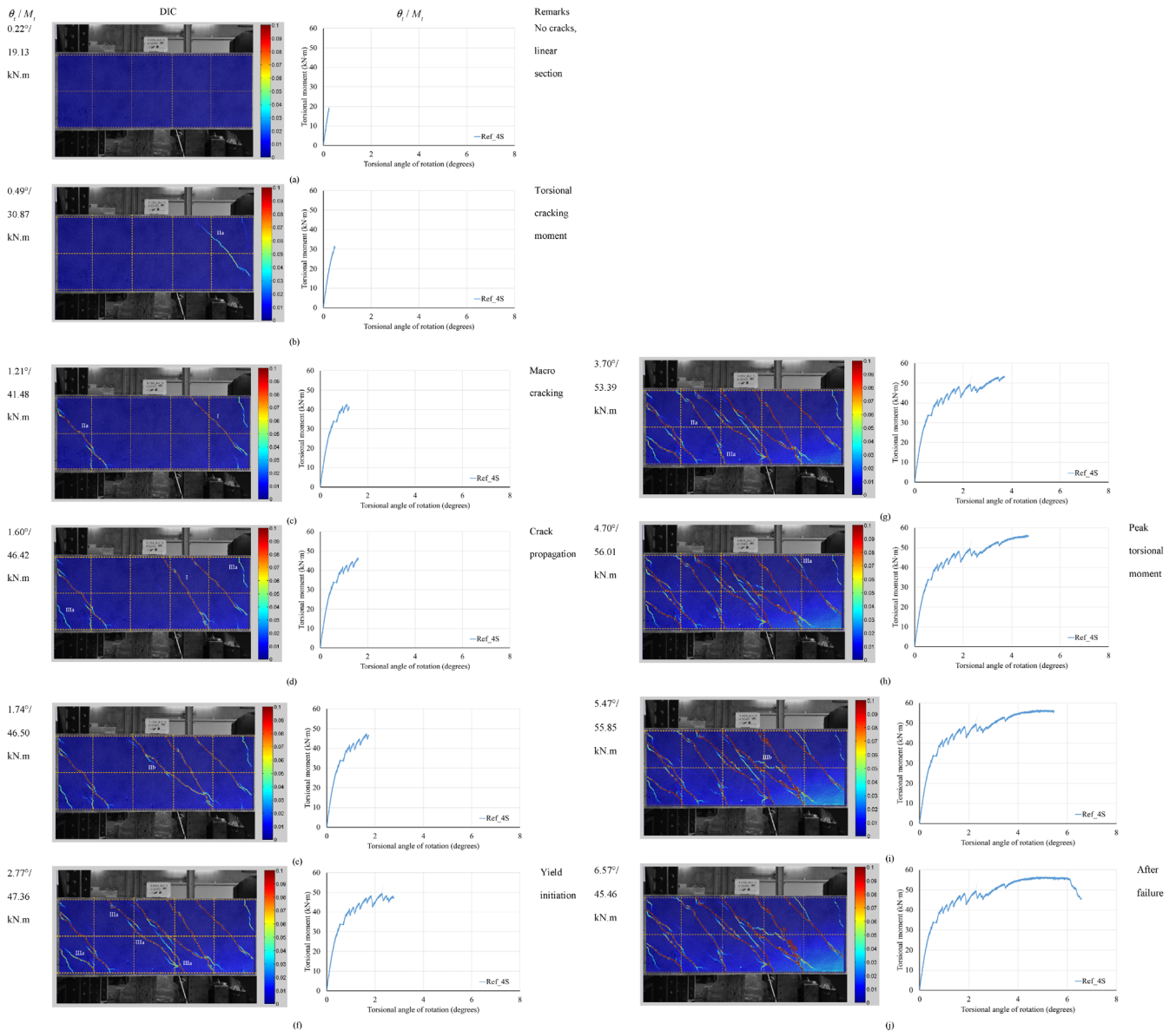
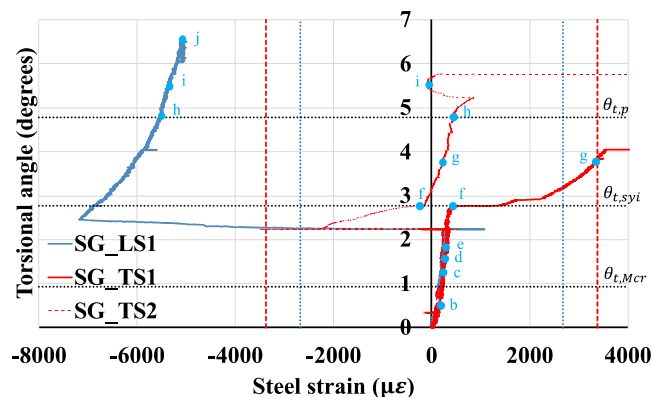


FIGURE 11 Cracking evolution of reference beam, Ref\_4S using digital image correlation (DIC)



**FIGURE 12** Steel strain versus torsional angle of rotation of reference beam, Ref\_4S

strain gauges are positioned close to the center of the beam (950 mm, Figure 4b). The beam then enters micro/macro crack propagation phase, shown in Figure 11c–e, at  $1.21^\circ$ ,  $1.60^\circ$  and  $1.74^\circ$  where several cracks are formed and the corresponding strains are shown in Figure 12 (points c, d and e). All the cracks formed at this stage, run almost throughout the respective beam faces, with limited breaks that is, cracks with branches or splitting cracks. This response is different from the strengthened beams (Figure 8b), which experience more cracks with many branches, due to the crack opening and slide resisting mechanisms provided by CFRP laminates bridging these cracks.

Figure 11f corresponds to the stage when yielding of steel reinforcement is registered and cracks are formed in the central study region, which is followed by a continuous degradation of the torsional resistance of the beam. A strain jump at this stage is registered, presented by point “f” in Figure 12. Corresponding to stages in between points “e” and “f,” two other strain gauges (SG\_LS1 and SG\_TS1) have registered a sudden abrupt increase in strains, due to crack process leading to the yielding of the respective reinforcements. The peak torsional moment is obtained at  $4.78^\circ$ ,  $56.68 \text{ kN}\cdot\text{m}$  and the DIC image closer to the value is presented in Figure 11h ( $4.70^\circ$ ,  $56.01 \text{ kN}\cdot\text{m}$ ), with the corresponding strain value at points “h” in Figure 12. Finally, the crack pattern of the beam’s failure is shown in Figure 11j. Comparing the after failure images of reference beam (Figure 11j) and strengthened beam S4F\_L4S5 (Figure 8k), it is notable the much higher number of cracks (smeared in the beam’s test zone) in S4F\_L4S5 due to the contribution of the CFRP laminates, leading to the increased torsional moment capacity.

### 3.2.4 | Additional results and outcome of DIC procedure

Figure 13 shows the surface strain distribution of all the tested beams where DIC was used. The CFRP laminates

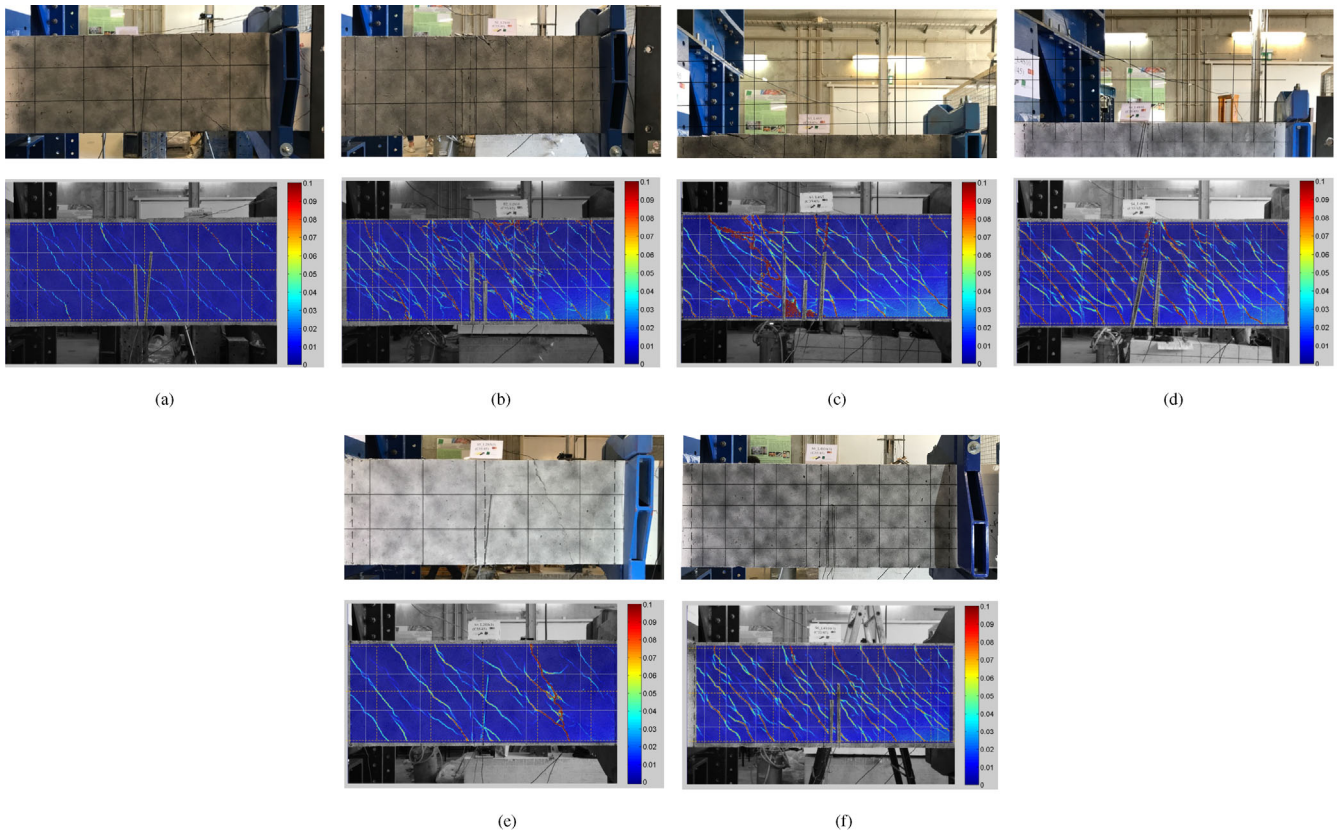
are represented by yellow dotted lines both in horizontal and longitudinal direction in the DIC images, and by black solid lines in the photographs of the specimens.

Figure 13a shows the DIC analysis of Beam S4F\_L2S5. Although failure in this beam was not captured by DIC, as it took place in a portion of the beam that was not monitored by the camera (see Figure 6a), the DIC images can be used to examine in greater detail both the crack development and evolution. An average crack spacing of 143 mm was calculated from the results of DIC considering only full cracks (Type I) on the left face, while the average crack spacing considering all four faces was 133 mm. A summary of the crack analysis is presented in Table 8 for all beams, including both values obtained from DIC, considering only the left face of the beam and overall visual and photographic inspection considering all the four faces at failure. The results show a small difference of 2.5% between the different techniques adopted for measuring crack spacing.

The DIC analysis of S4F\_L2S10, which was strengthened with twice the amount of transverse CFRP laminates than S4F\_L2S5, is shown in Figure 13b. Also in this case, the critical crack (Figure 6b) was not captured by DIC. A higher number of cracks formed along S4F\_L2S10 (average crack spacing of 120 mm) due to contribution of the extra percentage of transverse laminates that resulted in a higher torsional moment capacity. The failure pattern of beam S4F\_L4S5, which failed by CFRP rupture followed by concrete crushing on the top and left face, was successfully captured by DIC (Figure 13c). Figure 13d shows the crack pattern and strain field at failure of specimen S4F\_L4S10, which was strengthened with the highest amount of longitudinal and transverse reinforcement ratios and failed prematurely in the over-reinforced region at the loading end. Also in this case, the use of DIC enables a more detailed visualization and examination of secondary and tertiary cracks, successfully terminating the formation of spiral cracks and increasing the ductility performance of the strengthened beams. In few cases, it was also noticed that cracks developed along the CFRP reinforcement, although only at critical load levels (Figure 13c, top longitudinal CFRP laminate).

The average crack spacing in beam S3F\_L2S5, which failed by concrete crushing on the unstrengthened top surface (Figure 13e) and on the left face captured by DIC, was 186 mm, which is the largest that was observed in this study. Figure 13f shows the DIC analysis of beam S3F\_L4S10, which failed due to local crushing between the steel jackets on the top face, as for beam S4F\_L4S10.

Based on the results analyzed by DIC, the technique has helped in gaining a better understanding of:



**FIGURE 13** Digital image correlation (DIC) results: (a) S4F\_L2S5, (b) S4F\_L2S10, (c) S4F\_L4S5, (d) S4F\_L4S10, (e) S3F\_L2S5, and (f) S3F\_L4S10

**TABLE 8** Comparison of average crack spacing based on digital image correlation (DIC) and local measures

| Beam      | Average crack spacing according to DIC (mm):<br>Left face | Average crack spacing (mm):<br>All faces | DIC/average of four faces (%) |
|-----------|---|--|-------------------------------|
| Ref_4S    | 163.76  | 200.28                                   | 81.77                         |
| S4F_L2S5  | 142.86  | 132.59                                   | 107.75                        |
| S4F_L2S10 | 120.00  | 104.48                                   | 114.86                        |
| S4F_L4S5  | 139.58  | 133.33                                   | 104.69                        |
| S4F_L4S10 | 114.00  | 101.37                                   | 112.46                        |
| S3F_L2S5  | 186.07  | 169.20                                   | 109.97                        |
| S3F_L4S10 | 120.45  | 139.90                                   | 86.09                         |
| Average   |   |  | 102.51                        |

- The torsional crack evolution process in thin-walled elements strengthened with NSM CFRP laminates subjected to torsion;
- The interlinking of some secondary and tertiary cracks, has degenerated in to primary cracks, resulting in a smeared crack distribution pattern of the strengthened

beams at their failure stage. However in the case of reference beam, there is formation of many primary cracks (full cracks). Crossing the information of the crack propagation process by DIC with the strain evolution in the reinforcement systems has contributed for a deeper understanding of the contribution of the CFRP laminates for the torsional strengthening of the tested RC beams. This information can now be used for assessing the predictive performance of advanced computational models based on the finite element method. After calibrating with the help of this experimental information, these models can be used for executing parametric studies, not only for assessing the influence of relevant parameters on the strengthening performance of the adopted NSM technique, but also for assisting on the enhancement/development of design guidelines;

- The NSM strengthening technique increased not only the torsional load carrying capacity, but also the torsional ductility corresponding to the unstrengthened beams.

Even though, no premature failure at the extremities of the CFRP laminates were not observed, the anchorage



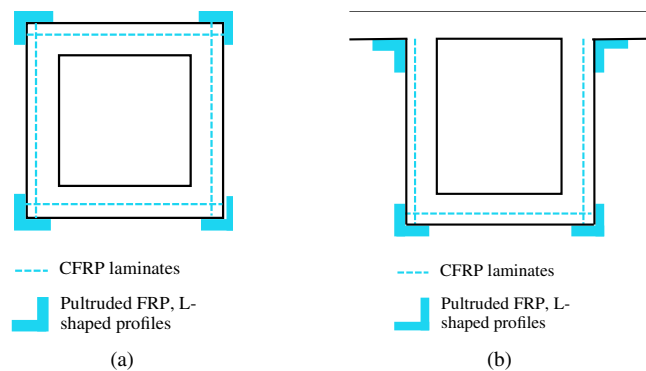


**FIGURE 14** Strategies (a and b) for improving the anchorage conditions for the extremities of near surface mounted carbon fiber reinforced polymer (NSM CFRP) laminates

conditions of these zones can be improved by providing pultruded L-shaped FRP profiles bonded by resin or by screws as shown in Figure 14.

### 3.2.5 | Strengthening assessment

The strengthening configurations of both series are verified against the formulations provided in the *fib* Bulletin 90.<sup>28</sup> Although, the code does not provide specific equations for NSM strengthening, the design procedure (Equation 5) follows the same procedure. First, the torsional resistance is evaluated using the average mean values of the material properties from the experimental tests. Second, the equations are used to design the beams, using design values (considering partial safety factors) from the experimental results.

$$T_{Rd} = \min(T_{Rd,s} + T_{Rd,f}, T_{Rd,max}) \quad (5)$$

$$T_{Rd,s} = 2A_k \frac{A_s}{S} f_{yd} \cot\theta \quad (6)$$

$$T_{Rd,f} = 2k_{fs} \frac{b_f t_f}{s_f} b h f_{fwd} \cot\theta \quad (7)$$

$$k_{fs} = 1 - e^{-a e^{-b \rho_w, eq}} \quad (8)$$

$$T_{Rd,max} = 2\nu \alpha_{cw} f_{cd} A_k t_{ef,i} \sin\theta \cos\theta \quad (9)$$

where  $T_{Rd}$  is the torsional resistance of the member,  $T_{Rd,s}$  is torsional resistance by transverse steel reinforcement (adopted from NTC-2018),  $T_{Rd,f}$  is the resistance by transverse CFRP reinforcement,  $T_{Rd,max}$  is the resistance by the diagonal compressive struts,  $A_k$  is the area enclosed by the center line of the connecting walls,  $A_s$  is the area

of the steel stirrups (only one leg is considered as the other leg does not offer resistance to the same component of shear flow),  $f_{yd}$  is the design yield strength,  $\theta$  is the diagonal compressive strut angle inclination,  $b_f$  and  $t_f$  are breadth and depth of the cross section of the FRP laminate,  $b$  and  $h$  are the breadth and depth of the beam cross section,  $f_{fwd}$  is the design value of the FRP strengthening contribution,  $s_f$  is the spacing of the FRP laminates,  $\nu$  is strength reduction factor for cracked concrete in shear,  $\alpha_{cw}$  is a coefficient taking into account the state of stress in compression chord,  $f_{cd}$  is the design compressive strength of concrete,  $t_{ef,i}$  is the effective wall thickness ( $A$  is the outer cross sectional area and  $u$  is the perimeter of the cross section). Available research shows (Chen et al.,<sup>13</sup> Dias and Barros,<sup>29</sup> Bianco et al.<sup>30</sup>) that by increasing the percentage of shear reinforcement, the contribution of FRP for the shear strengthening is detrimentally affected. This concept is now extended for the torsional strengthening by affecting the  $T_{Rd,f}$  by the  $k_{fs}$  factor that depends on the  $\rho_w, eq$  (Equation 8), which is the equivalent reinforcement ratio (Table 3). The  $a$  and  $b$  constants of this inverted sigmoid function were calibrated by the obtained results, but more experimental data will be necessary for a more reliable applicability of this parameter. The evaluation of the  $f_{fwd}$  was performed according to the formulation proposed by Bianco et al.,<sup>30</sup> whose parameters values are indicated in the footnote of Table 10 and the equations are presented in Appendix B.

The results of the evaluation are presented in Table 9 (using average values for the material parameters and unit values for partial safety factors) and the design values for the same are presented in Table 10. By using average values for the material properties a very good agreement with the experimental values was obtained ( $\frac{T_{Rd,exp}}{T_{Rd,num}} = 1.06$ ), while in case of design values a  $\frac{T_{Rd,exp}}{T_{Rd,num}} = 1.5$  was determined, which is a proper safety factor for structures that have failed with the yield initiation of the existing steel reinforcement.

Comparing the design values with the experimental results, for example, beam S4F\_L4S5, the updated predicted resistance is 27.71 kN·m, which corresponds to 35% of the peak experimental torsional moment (79.37 kN·m), 0.49° angle of rotation (corresponds to 6% of the experimental angle of rotation at peak moment), the experimental CFRP strain evolution is in the initial stages (Figure 9) and the crack pattern (Figure 8b) has very few primary and secondary cracks. The same pattern is observed in all the strengthened beams using NSM-CFRP laminates both in four face (Series 1) and three face (Series 2) retrofitting solutions.

Thus the increase in torsional moment carrying capacity and torsional angle of rotation, and the reduced crack pattern for the predicted and evaluated values according to *fib* Bulletin 90,<sup>28</sup> shows the increased performance of the experimentally tested beams.

**TABLE 9** Evaluation of the experimental results using *fib* bulletin 90<sup>28</sup>

| Beams     | $T_{Rd,s}$ (kN·m) | $T_{Rd,max}$ (kN·m) | $\rho_{w,eq}$ | $f_{fw}$ (MPa) | $k_{fs}$ | $T_{Rd,f}$ (kN·m) | $T_{Rd,num}$ (kN·m) | $T_{Rd,exp}$ (kN·m) | $\frac{T_{Rd,exp}}{T_{Rd,num}}$ |
|-----------|-------------------|---------------------|---------------|----------------|----------|-------------------|---------------------|---------------------|---------------------------------|
| Ref_4S    | 25.64             | 155.37              | 0.502         | -              | -        | -                 | <b>25.64</b>        | 56.69               | 2.2113                          |
| S4F_L2S5  | 25.64             | 155.37              | 0.573         | 2,346          | 0.906    | 47.59             | <b>73.23</b>        | 78.3                | 1.0693                          |
| S4F_L2S10 | 25.64             | 155.37              | 0.644         | 2,346          | 0.550    | 57.78             | <b>83.42</b>        | 81.69               | 0.9793                          |
| S4F_L4S5  | 25.64             | 155.37              | 0.573         | 2,346          | 0.906    | 47.59             | <b>73.23</b>        | 79.37               | 1.0839                          |
| S4F_L4S10 | 25.64             | 155.37              | 0.644         | 1982           | 0.550    | 48.82             | <b>74.45</b>        | 83.02               | 1.1150                          |
| S3F_L2S5  | 25.64             | 155.37              | 0.555         | 1982           | 0.955    | 31.81             | <b>57.44</b>        | 66.65               | 1.1602                          |
| S3F_L4S10 | 25.64             | 155.37              | 0.608         | 1982           | 0.749    | 49.89             | <b>75.53</b>        | 70.27               | 0.9304                          |
| Average   |                   |                     |               |                |          |                   |                     |                     | 1.0564                          |

Note:  $A_k = 90,000 \text{ mm}^2$ ,  $A_s = 100.53 \text{ mm}^2$ ,  $f_y = 566.70 \text{ MPa}$ ,  $\theta = 45^\circ$ ,  $s = 200 \text{ mm}$  (100 mm),  $b_f = 10 \text{ mm}$ ,  $t_f = 1.4 \text{ mm}$ ,  $b = h = 400 \text{ mm}$ ,  $f_{ck} = f_{cm} - 8 = 23.8 \text{ MPa}$ ,  $\nu = 0.6 \left(1 - \frac{f_{ck}}{250}\right) = 0.54$ ,  $\alpha_{cw} = 1$ ,  $f_{cm} = 31.8 \text{ MPa}$ ,  $t_{ef,i} = A/u = 400^2/1600 = 100 \text{ mm}$ .

**TABLE 10** Prediction of the experimental results using *fib* bulletin 90<sup>28</sup> considering design values and partial safety factors

| Beams     | $T_{Rd,s}$ (kN·m) | $T_{Rd,max}$ (kN·m) | $f_{fwd}$ (MPa) | $k_{fs}$ | $T_{Rd,f}$ (kN·m) | $T_{Rd,num}$ (kN·m) | $T_{Rd,exp}$ (kN·m) | $\frac{T_{Rd,exp}}{T_{Rd,num}}$ |
|-----------|-------------------|---------------------|-----------------|----------|-------------------|---------------------|---------------------|---------------------------------|
| Ref_4S    | 22.29             | 77.52               | -               | -        | -                 | <b>22.29</b>        | 56.69               | 2.543                           |
| S4F_L2S5  | 22.29             | 77.52               | 1,366           | 0.906    | 27.71             | <b>50.00</b>        | 78.3                | 1.566                           |
| S4F_L2S10 | 22.29             | 77.52               | 1,237           | 0.550    | 30.47             | <b>52.76</b>        | 81.69               | 1.548                           |
| S4F_L4S5  | 22.29             | 77.52               | 1,366           | 0.906    | 27.71             | <b>50.00</b>        | 79.37               | 1.587                           |
| S4F_L4S10 | 22.29             | 77.52               | 1,237           | 0.550    | 30.47             | <b>52.76</b>        | 83.02               | 1.574                           |
| S3F_L2S5  | 22.29             | 77.52               | 1,366           | 0.955    | 21.92             | <b>44.21</b>        | 66.65               | 1.507                           |
| S3F_L4S10 | 22.29             | 77.52               | 1,237           | 0.749    | 31.14             | <b>53.43</b>        | 70.27               | 1.315                           |
| Average   |                   |                     |                 |          |                   |                     |                     | 1.516                           |

Note:  $\gamma_s = 1.15$ ,  $f_{yd} = 492.78 \text{ MPa}$ ,  $\gamma_c = 1.5$ ,  $f_{cd} = 15.87 \text{ MPa}$ ,  $L_p = 21.4$ ,  $A_c = 25,000$ ,  $L_d = 800$ ,  $V_f^{lr} = 32,844$ ,  $f_{ctm} = 2.44$ ,  $E_c = 31,616$ ,  $J_1 = 0.000009$ ,  $C_3 = 1959$ ,  $L_{rfe} = 218.3$ ,  $V_{fi}^{bd} = 41.9$ ,  $L_{Rfi} = 100$ ,  $f_{ctm}^* = 1.39$ ,  $\partial_{Lu} = 0.6335$ ,  $\partial_{L1}(L_{Rfi}) = 0.6335$ ,  $A_2 = 16,764$ ,  $A_3 = 0.17$ ,  $\gamma_{max} = 0.0018$ ,  $V_{fi,eff}^{max} = 19,120$ .

## 4 | CONCLUSIONS

This paper discusses an experimental programme on torsional strengthening of thin walled tubular RC structures using different strengthening ratios of longitudinal and transversal CFRP laminates applied according to the NSM technique (in four and three strengthened faces). Based on the results obtained from the tests, the NSM CFRP strengthening in both longitudinal and transverse direction is a promising rehabilitation solution for torsional deficient RC structures. The technique increases the torsional moment carrying capacity of the beams depending on the CFRP reinforcement ratios. The NSM strengthening also increases the ductility performance of the strengthened element with respect to the corresponding unstrengthened element. The application of DIC technique provides useful data in understanding the contribution of CFRP laminates in resisting the applied torsional moment. Apart from these general conclusions, which include information extracted from DIC analysis, the following conclusions can be drawn.

- All four faces and three faces NSM CFRP strengthening schemes resulted in enhanced torsional

performance, with an increase in moment carrying capacity varying from 18 to 46% depending on the adopted strengthening ratios.

- Apart beam S3F\_L2S5, the strengthened beams exhibited higher ductility than the reference one, ranging from 19 to 76%.
- Four faces strengthened beams (Series 1) performed better than the three faces strengthened counterparts (Series 2), due to early failure of the unstrengthened top surface of the beams of Series 2.
- With the exception of beams S4F\_L4S10 and S3F\_L4S10, all other beams failed by CFRP rupture followed by concrete crushing. Beams S4F\_L4S10 and S3F\_L4S10 failed prematurely due to the development of high stresses around the steel loading section.
- DIC measurements provided evidence that the NSM CFRP laminates were effectively mobilized and assisted in controlling crack opening and reducing crack spacing (by about 15–49%). It was also shown that the crack opening behavior follows a sequence of typical steps: after an initial sudden displacement increment, crack opening increases very mildly, until right before failure when one of the cracks coalesce and suddenly suffers

strong displacement increments until failure. The sudden displacement jump that occurs at the moment when a new crack opens tends to be milder while deformation increases and damage accumulates, until failure. This information can be further explored to improve the methods for anticipating the collapse of structures based on the monitoring of existing cracks.

## ACKNOWLEDGMENTS

The first author would like to thank the Marie Curie Initial Training Network “Endure” MC-ITN-2013-607851, European Network for Durable Reinforcement and Rehabilitation Solutions, for the grant received to perform the research. Also, to the industries CASAIS and CiviTest in helping to execute the experimental work. The support provided by FCT through the PTDC/ECM-EST/1882/2014 project is also acknowledged.

## DATA AVAILABILITY STATEMENT

The raw/processed data required to reproduce these findings cannot be shared at this time as the data also forms part of an ongoing study.

## ORCID

Chandan C. Gowda  <https://orcid.org/0000-0002-3945-4814>

Joaquim A. O. Barros  <https://orcid.org/0000-0003-1528-757X>

## REFERENCES

- Alkhrdaji BT, Thomas J. Methods of upgrading concrete structures. *Concrete Repair Bulletin*. 2002;10–15.
- Emmons PH, Vaysburd AM, Thomas J. Strengthening concrete structures, Part I. *Concr Int*. 1998;19(3):53–58.
- Rodriguez M, Park R. Repair and strengthening of reinforced concrete buildings for seismic resistance. *Earthquake Spectra*. 1991;7(3):439–459.
- Panchacharam S, Belarbi A. Torsional behavior of reinforced concrete beams strengthened with FRP composites. *First FIB Congress on Concrete Structures in 21st Century; 2002, Osaka, Japan, Oct 13–19; 2002*. pp. 1–11.
- Deifalla A, Ghobarah A. Simplified analysis for torsionally strengthened RC beams using FRP. *Proceedings of International Symposium on Bond Behaviour of FRP in Structures (BBFS 2005); 2005 Dec 5–7; Hong Kong*.
- Hii AKY, Al-Mahaidi R. An experimental and numerical investigation on torsional strengthening of solid and box-section RC beams using CFRP laminates. *Compos Struct*. 2006;75(1–4): 213–221. <https://doi.org/10.1016/j.compstruct.2006.04.050>.
- Chalioris CE. Analytical model for the torsional behaviour of reinforced concrete beams retrofitted with FRP materials. *Eng Struct*. 2007;29(12):3263–3276. <https://doi.org/10.1016/j.engstruct.2007.09.009>.
- Deifalla A, Ghobarah A. Strengthening RC T-beams subjected to combined torsion and shear using FRP fabrics: Experimental study. *J Compos Constr*. 2010;14(3):301–311. [https://doi.org/10.1061/\(ASCE\)CC.1943-5614.0000091](https://doi.org/10.1061/(ASCE)CC.1943-5614.0000091).
- Al-Bayati G, Al-Mahaidi R, Kalfat R. Torsional strengthening of reinforced concrete beams using different configurations of NSM FRP with epoxy resins and cement-based adhesives. *Compos Struct*. 2017;168:569–581. <https://doi.org/10.1016/j.compstruct.2016.12.045>.
- Al-Bayati G, Al-Mahaidi R, Hashemi MJ, Kalfat R. Torsional strengthening of RC beams using NSM CFRP rope and innovative adhesives. *Compos Struct*. 2018;187:190–202. <https://doi.org/10.1016/j.compstruct.2017.12.016>.
- El-Saikaly G, Godat A, Chaallal O. New anchorage technique for FRP shear-strengthened RC T-beams using CFRP rope. *J Compos Constr*. 2015;19(4):1–11. [https://doi.org/10.1061/\(ASCE\)CC.1943-5614.0000530](https://doi.org/10.1061/(ASCE)CC.1943-5614.0000530).
- Chalioris CE, Kosmidou PMK, Papadopoulos NA. Investigation of a new strengthening technique for RC deep beams using carbon FRP ropes as transverse reinforcements. *Fibers*. 2018;6(3). <https://doi.org/10.3390/fib6030052>. [https://www.mdpi.com/2079-6439/6/3/52?type=check\\_update&version=1](https://www.mdpi.com/2079-6439/6/3/52?type=check_update&version=1)
- Dias SJ, Barros JAO. Shear strengthening of RC beams with NSM CFRP laminates: Experimental research and analytical formulation. *Compos Struct J*. 2013;99:477–490. <https://doi.org/https://doi.org/10.1016/j.compstruct.2012.09.026>.
- Bianco V, Barros JAO, Monti G. Bond model of NSM-FRP strips in the context of the shear strengthening of RC beams. *ASCE J Struct Eng*. 2009;135(6):619–631. [https://doi.org/10.1061/\(ASCE\)0733-9445\(2009\)135:6\(619\)](https://doi.org/10.1061/(ASCE)0733-9445(2009)135:6(619)).
- Choi S, Shah SP. Measurement of deformations on concrete subjected to compression using image correlation. *Exp Mech*. 1997;37(3):307–313. <https://doi.org/10.1007/BF02317423>.
- Fayyad TM, Lees JM. Application of digital image correlation to reinforced concrete fracture. *Procedia Mater Sci*. 2014;3(August): 1585–1590. <https://doi.org/10.1016/j.mspro.2014.06.256>.
- Pan B, Qian K, Xie H, Asundi A. Two-dimensional digital image correlation for in-plane displacement and strain measurement: A review. *Meas Sci Technol*. 2009;20(6):062001. <https://doi.org/10.1088/0957-0233/20/6/062001>.
- Chu TC, Ranson WF, Sutton MA. Applications of digital-image-correlation techniques to experimental mechanics. *Exp Mech*. 2006;25(3):232–244. <https://doi.org/10.1007/bf02325092>.
- Peters WH, Ranson WF. Digital imaging techniques in experimental stress analysis. *Opt Eng*. 1982;21(3):427–431.
- BS EN 12390-3:2009 Testing hardened concrete - Part 3: Compressive strength of test specimens. *British Standard. Series volume 3, issue 1*. Pages 420–457.
- EN\_10002-1 (1990). (2001). *Metallic materials tensile testing part 1: Method of test at ambient temperature*. European Committee for Standardization (CEN). Available from: <http://scholar.google.com/scholar?hl=en&btnG=Search&q=intitle: Metallic+Materials+-+Tensile+Testing+-+Part+1:+Method+of+test+at+ambient+temperature#9>
- ISO, 527-5. *Plastics—Determination of tensile properties - Part 5: Test conditions for unidirectional fibre-reinforced plastic composites*. International Organisation for Standardization (ISO); 1997, Geneva, Switzerland (Vol. 1). Available from: [http://www.chemshow.cn/UploadFile/datum/1000/huayangyq2008w\\_2009420145250792688.pdf](http://www.chemshow.cn/UploadFile/datum/1000/huayangyq2008w_2009420145250792688.pdf)
- Gowda CC, Barros JAO, Guadagnini M. Experimental study of torsional strengthening on thin walled tubular reinforced

- concrete structures using NSM-CFRP laminates. *Compos Struct.* 2018;208(July 2018):585–599. <https://doi.org/10.1016/j.compstruct.2018.10.050>.
24. ACI Committee. Guide for the design and construction of externally bonded FRP systems for strengthening existing structures (ACI 440.2R-08); 2008.
  25. Gowda CC, Barros JAO. Exploring NSM technique for torsional strengthening of tubular type RC structures. *Proceedings of the 11th fib International PhD Symposium in Civil Engineering.* University of Tokyo; 2016, August, Tokyo, Japan. pp. 1–8.
  26. Gowda CC, Barros JAO, Guadagnini M. Experimental investigation on torsional strengthening of box RC structures using NSM FRP. *9th International Conference on Fibre-Reinforced Polymer (FRP) Composites in Civil Engineering (CICE 2018); 2018 Jul 17–19, Paris, France.*
  27. Chaliotis CE, Karayannis CG. Effectiveness of the use of steel fibres on the torsional behaviour of flanged concrete beams. *Cem Concr Compos.* 2009;31(5):331–341. <https://doi.org/10.1016/j.cemconcomp.2009.02.007>.
  28. *fib Bulletin* 90. T.G. 5.1. Externally applied FRP reinforcement for concrete structures; 2019.
  29. Chen GM, Teng JG, Chen JF. Shear strength model for FRP-strengthened RC beams with adverse FRP-steel interaction. *J Compos Constr.* 2013;17(1):50–66. [https://doi.org/10.1061/\(ASCE\)CC.1943-5614.0000313](https://doi.org/10.1061/(ASCE)CC.1943-5614.0000313).
  30. Bianco V, Monti G, Barros JAO. Design formula to evaluate the NSM FRP strips shear strength contribution to a RC beam. *Compos Part B Eng.* 2014;56:960–971. <https://doi.org/10.1016/j.compositesb.2013.09.001>.

## AUTHOR BIOGRAPHIES



**Chandan C. Gowda**, Researcher, ISISE, Department of Civil Engineering, University of Minho, 4800-058 Guimaraes, Portugal. Email: [chandu627@gmail.com](mailto:chandu627@gmail.com).



**Joaquim A. O. Barros**, Full Professor ISISE, Institute of Science and Innovation for Bio-Sustainability (IB-S), Department of Civil Engineering, University of Minho, 4800-058 Guimaraes, Portugal. Email: [barros@civil.uminho.pt](mailto:barros@civil.uminho.pt).



**Maurizio Guadagnini**, Senior Lecturer, Department of Civil and Structural Engineering, The University of Sheffield, Sir Fredrick Mappin building, Mappin Street, Sheffield, UK S1 3JD. Email: [m.guadagnini@sheffield.ac.uk](mailto:m.guadagnini@sheffield.ac.uk).

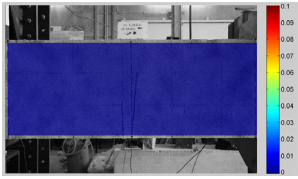
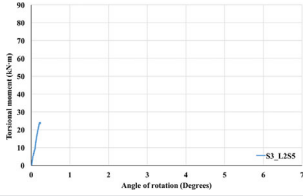
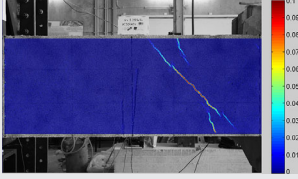
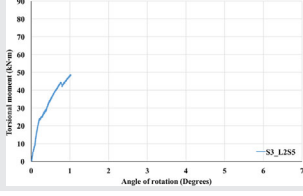
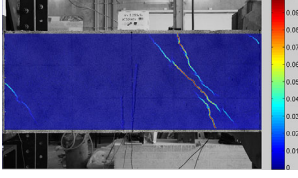
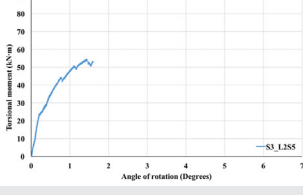
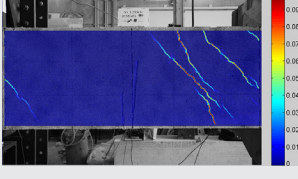
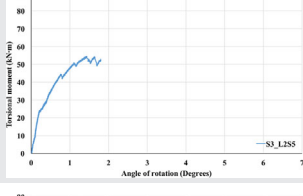
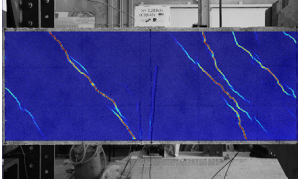
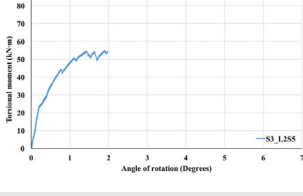
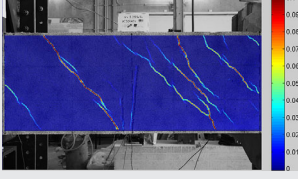
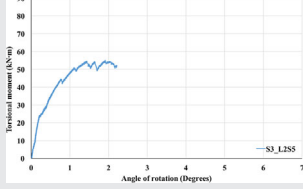
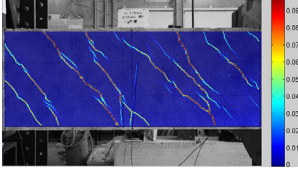
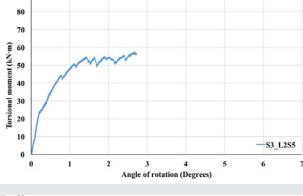
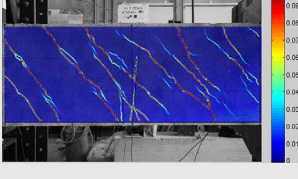
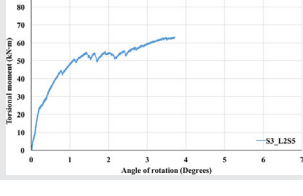


**Eduardo Pereira**, Assistant Professor, ISISE, Department of Civil Engineering, University of Minho, 4800-058 Guimaraes, Portugal. Email: [eduardo.pereira@civil.uminho.pt](mailto:eduardo.pereira@civil.uminho.pt).

**How to cite this article:** Gowda CC, Barros JAO, Guadagnini M, Pereira E. Torsional strengthening of tubular type RC beams with NSM technique: Structural performance and cracking process using DIC. *Structural Concrete.* 2020;1–23. <https://doi.org/10.1002/suco.202000174>

APPENDIX A

Beam S3F\_L2S5 (three face strengthening): Step by step DIC analyses

| $\theta_t/M_t$   | DIC   | $\theta_t - M_t$   | Remarks   |
|------------------|---|--|---|
| 0.34°/27.56 kN·m |    |    | No cracks, linear section   |
| 1.02°/48.19 kN·m |    |    | Torsional cracking moment   |
| 1.59°/53.26 kN·m |    |    | Macro cracking phase  |
| 1.79°/52.63 kN·m |   |   | Micro cracking phase  |
| 1.97°/53.99 kN·m |  |  | Crack propagation phase   |
| 2.20°/51.80 kN·m |  |  | Crack propagation phase   |
| 2.72°/56.30 kN·m |  |  | Termination of crack propagation phase and initiation of steel yielding phase |
| 3.70°/63.08 kN·m |  |  | Steel yielding phase  |

(Continues)

| $\theta_t/M_t$      | DIC | $\theta_t - M_t$ | Remarks                                    |
|---------------------|-----|------------------|--|
| 5.28°/59.84<br>kN·m |     |                  | Steel yielding phase                       |
| 5.16°/61.41<br>kN·m |     |                  | Peak torsional moment, followed by failure |
| 5.82°/57.14<br>kN·m |     |                  | End of test                                |

## APPENDIX B

According to BSMCFT, the design value of tensile strength in FRP laminates by NSM technique ( $f_{fwd}$ ) is evaluated by  $f_{fwd} = \frac{V_{fi,eff}^{max}}{a_f t_f}$

where

$V_{fi,eff}^{max} = V_{fi,eff}(\gamma_{max}) = \frac{\delta_1 A_2}{2L_d A_3 \gamma_{max}} \left[ \frac{\pi}{2} - \arcsin \psi - \psi \sqrt{1 - \psi^2} \right]$ , to obtain all the constants and unknowns, the following equations are necessary. More details on the BSMCFT is available in Bianco, Monti and Barros.<sup>30</sup>

1. Evaluation of constants, including geometric constants, mechanical constants and bond-modeling constants;

a. The geometric constants are: effective perimeter of FRP laminate cross section ( $L_p$ ); cross sectional area of the prism surrounding the concrete ( $A_c$ ); and length of the CDC ( $L_d$ ).

$$L_p = 2(a_f + b_f) = 21.40; \quad A_c = s_w \frac{b_w}{2} = 25000;$$

$$L_d = \frac{h_w}{\sin \theta_v} = 800$$

b. The mechanical constants are: FRP laminate tensile strength; concrete tensile strength ( $f_{ctm}$ ); and Young's modulus ( $E_c$ ).

$$V_f^{tr} = a_f b_f f_{fu} = 32844; \quad f_{ctm} = 1.4 \left( \frac{f_{cm} - 8}{10} \right)^{2/3}$$

$$E_c = 2.15 \times 10^4 \left( \frac{f_{ctm}}{10} \right)^{2/3} = 2.50; = 31616.53$$

$f_{fu}$  is the tensile strength of the FRP laminate and  $f_{ctm}$  is the concrete tensile strength.

c. The bond-modeling constants are: bond modeling constant; integration constant ( $C_3$ ); constant of differential equation ( $\lambda$ ); effective resisting bond length ( $L_{Rfe}$ ); and corresponding maximum bond force ( $V_{f1}^{bd}$ ).

$$J_1 = \frac{L_p}{A_f} \left[ \frac{1}{E_f} + \frac{A_f}{A_c E_c} \right] \quad C_3 = \frac{V_f^{tr} J_1}{L_p \lambda}, \quad \frac{1}{\lambda^2} = \frac{\delta_1}{\tau_b J_1}$$

$$tL_{Rfe} = \frac{\pi}{2\lambda} = 215.81; = 0.000009; = 1959.13;$$

$$V_{f1}^{bd} = \frac{L_p \lambda \delta_1}{J_1} = 41.91$$

d. Evaluation of reduction factor ( $\eta$ ) and equivalent average resisting bond length ( $\bar{L}_{Rfi}^{eq}$ );

$$\bar{L}_{Rfi}^{eq} = \eta \bar{L}_{Rfi}$$

where

$$\bar{L}_{Rfi} = \frac{h \sin \theta_v (\cot \theta_v + \cot \beta)}{4 \sin(\theta_v + \beta)} = 100$$

$$\eta = \begin{cases} \frac{f_{ctm}}{f_{ctm}^*} & \text{if } f_{ctm} < f_{ctm}^* \\ 1 & \text{if } f_{ctm} > f_{ctm}^* \end{cases}$$

$$f_{ctm}^* = \frac{L_p \lambda \delta_1 \sin(\lambda L_{Rfi})}{J_1 \cdot \min(L_{Rfi} \tan \alpha, b_v/2) \cdot \min(s_f \sin \beta, 2L_{Rfi} \tan \alpha)} = 1.39$$

In which  $L_{Rfi}$  should be

$$L_{Rfi} = \begin{cases} \bar{L}_{Rfi} & \text{if } \bar{L}_{Rfi} \leq L_{Rfe} \\ L_{Rfe} & \text{if } \bar{L}_{Rfi} > L_{Rfe} \end{cases}$$

- e. Assessment of the imposed end slip value ( $\delta_{Lu}$ ), for which the maximum force  $V_{fi}(\bar{L}_{Rfi}^{eq}, \delta_{Li})$  in the constitutive law for the corresponding bond length  $\bar{L}_{Rfi}^{eq}$  is achieved;

$$\delta_{Lu} = \begin{cases} \delta_{Li}(\bar{L}_{Rfi}^{eq}) & \text{if } V_{fi}^{bd} < V_f^{tr} \\ \min[\delta_{Li}(\bar{L}_{Rfi}^{eq}); \delta_{Li}(V_f^{tr})] & \text{if } V_{fi}^{bd} \geq V_f^{tr} \end{cases} = 0.6335$$

where

$$\delta_{Li}(\bar{L}_{Rfi}^{eq}) = \begin{cases} \delta_1 [1 - \cos(\lambda \bar{L}_{Rfi}^{eq})] & \text{if } \bar{L}_{Rfi}^{eq} \leq L_{Rfe} \\ \delta_1 & \text{if } \bar{L}_{Rfi}^{eq} > L_{Rfe} \end{cases} = 0.6335$$

$$\delta_{Li}(V_f^{tr}) = \delta_1 \left\{ 1 - \cos \left[ -\arcsin \frac{C_3}{\delta_1} \right] \right\}$$

- f. Evaluation of the maximum effective capacity of the NSM FRP laminate ( $V_{fi,eff}^{max}$ ) with equivalent average resisting bond length ( $\bar{L}_{Rfi}^{eq}$ );

$$V_{fi,eff}^{max} = V_{fi,eff}(\gamma_{max}) = \frac{\delta_1 A_2}{2L_d A_3 \gamma_{max}} \left[ \frac{\pi}{2} - \arcsin \psi - \psi \sqrt{1 - \psi^2} \right] = 19120$$

where

$$A_2 = \frac{L_p \lambda}{J_1}; A_3 = \frac{\sin(\theta_v + \beta)}{2\delta_1}; \gamma_{max} = \frac{2\delta_{Lu}}{L_d \sin(\theta_v + \beta)} \quad \begin{matrix} A_2 = 16764.58, \\ A_3 = 0.1732, \\ \gamma_{max} = 0.0018 \end{matrix}$$

$$\psi = (1 - A_3) \gamma_{max} L_d = 0.75$$